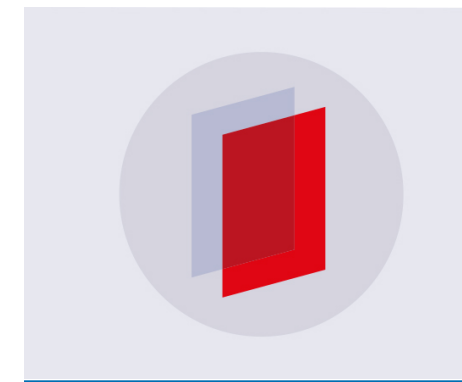
#### **PAPER**

### A general framework for photoionization calculations applied to nonthermal gas discharges in air

To cite this article: R Janalizadeh and V P Pasko 2019 Plasma Sources Sci. Technol. 28 105006

View the article online for updates and enhancements.





## IOP ebooks™

Bringing you innovative digital publishing with leading voices to create your essential collection of books in STEM research

Start exploring the collection - download the first chapter of every title for free.

Plasma Sources Sci. Technol. 28 (2019) 105006 (17pp)

https://doi.org/10.1088/1361-6595/ab4374

# A general framework for photoionization calculations applied to nonthermal gas discharges in air

R Janalizadeh<sup>1</sup> and V P Pasko

Communications and Space Sciences Laboratory, Department of Electrical Engineering, The Pennsylvania State University, University Park, PA 16802, United States of America

E-mail: reza.j@psu.edu and vpasko@psu.edu

Received 29 April 2019, revised 30 August 2019 Accepted for publication 11 September 2019 Published 17 October 2019



#### **Abstract**

A general framework for photoionization rate calculations in a constant pressure gaseous medium is introduced. The formulation includes the number of photons emitted per unit volume per unit time per unit wavelength due to a radiating source, photobasorption cross sections and density of species comprising the medium, and the photoionization probability (i.e. photoionization yield) of the species being photoionized. We derive a standard integral representation of the photoionization problem that may be readily converted to a set of Helmholtz differential equations for efficient calculation of the photoionization rate. The model is applied to the photoionization problem in air in which  $b^1 P_u$ ,  $b \not\in S_u^+$ ,  $c_3^1 P_u$ ,  $o_3^1 P_u$ ,  $c_4 \not\in S_u^+$  singlet states of N<sub>2</sub> are excited due to collisions with electrons generated as a result of nonthermal discharges. Radiative decay from these states gives rise to respective band systems Birge-Hopfield I, Birge-Hopfield II, Worley-Jenkins, Worley, and Carroll-Yoshino, and to photons which are generally energetic enough to ionize O<sub>2</sub>. The excitation rates and contribution of each band system to photoionization of O<sub>2</sub> in air are calculated for the first time. Using recently measured electron impact excitation cross sections of these states, and the recently measured extreme ultraviolet (XUV) spectra of N<sub>2</sub>, we quantify the emission from each singlet state. Absorption of emission is modeled using measured photoabsorption cross sections of N<sub>2</sub> and O<sub>2</sub>. The photoionization rate of O<sub>2</sub> upon absorption of a photon with a certain energy is calculated using experimental values for the photoionization yield of O<sub>2</sub>. Finally, we introduce a set of coefficients which define the differential representation of the problem of photoionization in air. The developed modeling framework allows accurate solution of photoionization problems in air for the broad range  $10^{-2} < p_{O_2}R < 10^4$  Torr cm, where  $p_{O_2}$  is the partial pressure of  $O_2$  in air in units of Torr ( $p_{O_2}$  = 152 Torr at atmospheric pressure) and R in cm is a characteristic spatial dimension of the system of interest. The model performance is demonstrated using a set of artificial sources leading to photoionization over a representative range of  $p_{O_2}R$  values and a realistic problem of dynamics of a double-headed streamer in air that was used in previous photoionization literature. The validity of the modeling framework is demonstrated by comparisons with the photo-ion yield function in air,  $Y(p_0,R)$ , derived from the classic photoionization model of Zheleznyak et al (1982) and more recent experimental data on photoionization in air.

Keywords: photoionization model, air, molecular oxygen, photoabsorption cross section, streamer discharge, ultraviolet radiation, singlet ungerade states of molecular nitrogen

0963-0252/19/105006 + 17\$33.00

© 2019 IOP Publishing Ltd

Author to whom correspondence should be addressed.

#### 1. Introduction

The molecular nitrogen, N2 is the main source of ultraviolet radiation in air with the strongest dipole-allowed radiative transitions occurring in the extreme ultraviolet (XUV), i.e. 80 -135 nm (e.g. Vallance-Jones 1974, p. 90, 135). The main excited electronic states of N<sub>2</sub> generating photons with wavelengths in this regime are the singlet *ungerade* states  $b^1 P_u$ ,  $b \not\in S_u^+$ ,  $c_3{}^1\mathsf{P}_u$ ,  $o_3{}^1\mathsf{P}_u$ , and  $c_{\mu}\mathsf{S}_u^+$  (e.g. Lofthus and Krupenie 1977) where the first two are of valence type and the last three are each the lowest member of a Rydberg series (see e.g. Heaves et al 2014). These photons are absorbed in air by both N2 and the molecular oxygen, O<sub>2</sub>. While the photoabsorption cross section of O<sub>2</sub> covers the entire XUV spectrum, the photoabsorption cross section of N<sub>2</sub> is significantly reduced for wavelengths longer than 98.5 nm (e.g. Hudson 1971). This reduction is due to the fact that in low current nonthermal plasmas in air, e.g. streamer discharges, practically all N<sub>2</sub> molecules are residing in the lowest vibrational level of the ground state, i.e.  $X^1S^+_{\sigma}(n\mathbb{X}^{\frac{1}{2}})$ . These molecules begin to absorb radiation with wavelengths / 398.5 nm, with 98.5 nm corresponding to the energy difference between the lower vibrational levels of the ground state and the aforementioned singlet states of N<sub>2</sub>. The electron impact collisions effectively populate vibrational levels  $n_{ij}$  of these singlet states and the resultant  $n \notin \mathbb{M}$   $n \in \mathbb{M}$  transitions between these states and the ground state create radiation with wavelengths / 398.5 nm that is not absorbed by N<sub>2</sub>. As a result, photons with wavelengths longer than 98.5 nm get absorbed only by O<sub>2</sub> and the fraction with wavelengths in between 98.5 and 102.5 nm (ionization threshold of O2) ionize O2. This phenomenology has been discussed extensively in (Zheleznyak et al 1982) and represents a fundamental mechanism of photoionization in air. As a result, absorption of XUV radiation in air may be described using 3 wavelength band regimes: (i) the emissions with wavelengths shorter than 98.5 nm which are extensively absorbed due to the aggregate photoabsorption effect of both N2 and O2, (ii) the emissions in the 98.5-102.5 nm interval which get exclusively absorbed by O2 and may consequently contribute to its photoionization, and (iii) the emissions with wavelengths longer than 102.5 nm, which still get absorbed by O2, but are not energetic enough to cause photoionization of  $O_2$ .

Zheleznyak et al (1982) introduced the currently most widely used photoionization model in air based on the phenomenology described above. In the current literature, photoionization calculations in air are performed using integral (e.g. Liu and Pasko 2004, and references therein) or differential (Bourdon et al 2007, and references therein) representations of this model. In particular, the differential representation provides considerable improvements with regards to the implementation efficiency of the model. Nevertheless, to the best knowledge of the authors, this paper is the first attempt to introduce a general framework for photoionization calculations, based on first principles and usage of experimental data. The presented framework can be readily adopted to quantify photoionization of any component of a gas mixture due to emission from an arbitrary band system (see e.g. Pasko 2018, Janalizadeh and Pasko 2019a, 2019b). This is of particular importance for quantifying photoionization of O2 in air. Since the model of Zheleznyak *et al* (1982) was first introduced, (i) extensive measurement data for the photoabsorption cross sections of  $N_2$  and  $O_2$  have been published (see e.g. Fennelly and Torr 1992, Keller-Rudek *et al* 2013), (ii) high resolution measurements of the emission spectra of  $N_2$  have been reported (Ajello *et al* 1989, James *et al* 1990, Heays *et al* 2014), and (iii) electron impact excitation cross sections of the aforementioned singlet states have been recently measured (Itikawa 2006, Malone *et al* 2012).

More recent photoionization models have benefited from these data. However, the accurate quantification of photoionizing radiation due to a nonthermal gas discharge in air is not yet complete. Stephens et al (2016) study the formative stage of a low temperature plasma where the electric field E is approximately equal to the breakdown electric field  $E_k$ . On the other hand, the electric field in the streamer head region may be on the order of  $5E_k$  (see figure 7(b)) which results in a significantly different electron energy distribution function and represents a separate stage in the discharge with significantly different time dynamics. Furthermore, Stephens molecular nitrogen generating photons (of the Carroll-Yoshino band system) capable of ionizing O2. In case of streamer propagation, Xiong and Kushner (2014) assign such photons to the Birge-Hopfield I and II band systems of N<sub>2</sub>. In general, the majority of observed XUV emissions from N2 are due to least-predissociated vibrational levels of  $b^1 P_u$ ,  $b \not\in S_u^+$ ,  $c \not\in S_u^+$  in addition to a comparable amount of emission from the decay of excited atomic dissociation products for sufficiently energetic electron collisions (Heays et al 2014). Also, emissions from  $c_3^{1}P_u$  and  $o_3^{1}P_u$  are not readily observed as they are strongly predissociated. This conclusion is based on emission cross section measurements (see e.g. James et al 1990, Ajello et al 2007). However, as stated in (Malone et al 2012) optical emission is too weak to be used for cross section measurements and methods such as electron energy loss (EEL) spectroscopy are superior (see e.g. Khakoo et al 2008, Heavs et al 2012). Also, Roncin and Launay (1998) have observed emissions from vibrational levels of both  $c_3^1 P_u$  and  $o_3^1 P_u$ which as stated by Malone et al (2012) may call for adjustments to the 100% predissociation yields of  $c_3^1 P_u$  and  $o_3^1 P_u$ stated in (e.g. Ajello et al 2007). Still, note that emission cross sections measured for  $c_3^1 P_u$  and  $o_3^1 P_u$  states of  $N_2$  as a result of 100 eV electron impact excitation are approximately 2 orders of magnitude less than  $c_{\mu} S_{u}^{+}$  which has the highest emission cross section among all states considered here (Heavs et al 2014). Also, the fact that measurements by Heavs et al (2014) have been performed under optically thin conditions (i.e. 2  $\mu$ Torr) implies that at higher pressures such weak emissions may get even more suppressed. Nevertheless, they may still contribute to further understanding of gas discharge phenomena at low air pressures, e.g. sprites which occur at low air densities at high altitudes in the Earth's atmosphere (see e.g. Pasko et al 2013, and references therein). Note that the quenching pressure for the various rovibrational levels of singlet states considered here covers a wide range. This is due to significantly different lifetimes of the rovibrational levels (starting from tens of picoseconds to few nanoseconds) (see e.g. Sprengers 2006, and references therein).

This is also the case for the predissociation yield of these levels. Since the quenching pressures for such levels are not yet available in the existing literature, the modeling studies of emissions from these levels in high pressure conditions have been impeded.

The modeling approach introduced in (Ségur et al 2006, Luque et al 2007) and further elaborated in (Bourdon et al 2007) through which the integral representation of the solution to the photoionization problem provided in (Zheleznyak et al 1982) is converted to a set of Helmholtz differential equations is the other important factor calling for introduction of a general framework for quantifying photoionization. Once the solution to the photoionization problem is expressed in a certain integral form (see section 2.1), the differential representation of the problem may be readily obtained (see section 2.2) and subsequently solved in a much more efficient manner. As a result, the purpose of the general framework for photoionization may be summarized as follows: deriving an integral representation similar to the form expressed in (e.g. Zheleznyak et al 1982, Liu and Pasko 2004, Bourdon et al 2007) and applying the approach introduced in (Ségur et al 2006, Luque et al 2007, Bourdon et al 2007) to convert the integral format of the solution to a set of Helmholtz differential equations. As will be demonstrated in this work, the only components necessary to achieve this goal for any photoionization problem are (i) the number of photons emitted per unit volume per unit time per unit wavelength from an emitting source, (ii) photoabsorption cross section and density of any component present in the medium, and (iii) the photoionization probability, i.e. photoionization yield of the gas component for which we wish to solve the photoionization problem.

In this paper, we solve the problem of  $O_2$  photoionization in air in terms of the above mentioned general photoionization framework. In section 2, we introduce the general framework for photoionization calculations in an arbitrary gaseous medium and in section 3, we apply the framework to the problem of photoionization of  $O_2$  due to nonthermal gas discharges in air. In section 4.1, we compare our model with the model of Zheleznyak *et al* (1982), outline the limitations of this model, and discuss corresponding improvements introduced in the present work. Section 4 concludes with simulation results for a streamer discharge and examination of the photo-ion yield function in air. We emphasize that the formulation developed in this work may be beneficial to efficient calculations of photoionization of other species in gaseous media (i.e. not only  $O_2$  in air).

#### 2. General photoionization framework

#### 2.1. Integral formulation

The rate of photoionization (i.e. number of photoionization events per unit volume per unit time with units cm<sup>-3</sup> s<sup>-1</sup>) of a species with density  $n_{\rm ion}$ , photoionization cross section  $\mathbf{s}_{\rm pa}$ , photoionization cross section  $\mathbf{s}_{\rm pa}$ , photoionization yield  $\mathbf{x}_{\rm ion} = \mathbf{s}_{\rm ion}/\mathbf{s}_{\rm pa}$ , located at position r due to a source comprised of volumetric elements  $\mathrm{d}V_{\mathrm{s}}$  located at  $r_{\mathrm{s}}$  is given by (e.g.

Zheleznyak et al 1982):

$$S_{\mathrm{ph}}(P) = \grave{Q}_{\phi} \grave{Q}_{\phi} e(P, P) e^{-k_{\mathrm{pa}_{r}}(P)|\stackrel{\mathcal{M}}{p}_{x}} r^{\mathcal{M}})$$

$$\frac{s_{\mathrm{pa}}(P)}{4\rho|P, P} r^{\mathcal{M}}_{\mathrm{ion}}(P) n_{\mathrm{ion}}(P) dV dV dV. \tag{1}$$

The quantity  $e(f \not\in I \phi)$  denotes number of photons emitted isotropically in all directions per unit volume per unit time per unit wavelength and  $k_{pa_i} = a_{j=1} k_{pa_i}$  is the total photabsorption coefficient of a medium comprised of several species each with photoabsorption coefficient  $k_{pa_j} = s_{pa_j} n_j$ , where  $n_j$  and  $s_{pa_j}$ denote the density and photoabsorption cross section of the jth species, respectively. The formulation (1) assumes constant densities of  $n_i$  and  $n_{ion}$  and therefore applies only to constant pressure conditions. The equation (1) states that from all the photons with wavelength  $\lambda$ , emitted from r, only the fraction  $e^{-k_{pa_r}(l)}|^{\frac{|X|}{2}}r^{\frac{|X|}{2}}$  reaches r. The rest get absorbed along the way. The probability that at point r (i.e. distance  $R = |R| = |r|^{\frac{|X|}{2}}$ from  $\frac{1}{1}$ , a photon gets absorbed by a single atom/molecule per unit volume of the species under investigation for photoionization is  $s_{pa}/(4pR^2)$  and the probability of photoionization upon photo absorption is denoted by  $\xi_{\text{ion}}$ . In practice it is convenient to express the photoionization rate (1) per one atom/molecule of the photoionized species per unit volume. We use notation  $S_{ph_1}(r)$ for this quantity. The photoionization rate for any density of photoionized species can then be calculated by simple multiplication of  $S_{ph}(r)$  by the density of these species, i.e.  $S_{ph}(r) = n_{ion}(r)S_{ph_1}(r)$ . The main focus of this section is to provide a framework to calculate  $S_{ph_1}(r)$  for the configuration specified above.

The source of radiation can be represented by M pairs  $(I_m(r, s_m(I)))$  for m = 1, 2, ..., M. The quantities  $I_m(r, s_m(I))$  and  $s_m(\lambda)$  denote the number of photons emitted per unit volume per unit time and the spectra of the mth emission, respectively. We note that the mth emission refers to an entire band system. For instance, in case of photoionization of  $O_2$  in air, each individual emission band system of  $N_2$  described in the previous section may be characterized by such a pair. Consequently, the source of radiation may be expressed as a superposition of individual elements in the form

$$\mathbf{e}(\mathbf{F}, \mathbf{F}, \mathbf{I}) = \mathbf{a}_{m=1}^{M} \mathbf{e}_{m}(\mathbf{F}, \mathbf{I}) = \mathbf{a}_{m=1}^{M} I_{m}(\mathbf{F}, \mathbf{F}, \mathbf{S}_{m}(\mathbf{I})), \qquad (2)$$

where  $s_m(\lambda)$  is normalized for all m as  $\grave{Q}_{\psi} s_m(l) \not \in 1$  and  $I_m(l) = \grave{Q}_{\psi} e_m(l) \not \in 1$  (1). Having substituted (2) into (1), we arrive at

$$S_{\text{ph}_{1}}(\vec{r}) = \overset{M}{\underset{m=1}{a}} S_{\text{ph}_{1m}}(\vec{r}) = \overset{M}{\underset{m=1}{a}} \grave{Q}_{V_{\varphi}} I_{m}(\vec{r}) \frac{\mathbb{W}}{2} \frac{g_{m}(pR)}{4pR^{2}} dV_{\varphi}$$
(3)

where

$$g_m(pR) = \grave{Q}_{\phi} s_m(I \not \Phi e^{-k_{\mathrm{pa}_r}(I \not \Phi R)} s_{\mathrm{pa}}(I \not \Phi t_{\mathrm{ion}} I \not \Phi d \not \Phi e^{-k_{\mathrm{pa}_r}(I \not \Phi R)} s_{\mathrm{pa}}(I \not \Phi t_{\mathrm{ion}} I \not \Phi d \not \Phi e^{-k_{\mathrm{pa}_r}(I \not \Phi R)} s_{\mathrm{pa}}(I \not \Phi t_{\mathrm{ion}} I \not \Phi d \not \Phi e^{-k_{\mathrm{pa}_r}(I \not \Phi R)} s_{\mathrm{pa}}(I \not \Phi t_{\mathrm{ion}} I \not \Phi d \not \Phi e^{-k_{\mathrm{pa}_r}(I \not \Phi R)} s_{\mathrm{pa}}(I \not \Phi t_{\mathrm{ion}} I \not \Phi d \not \Phi e^{-k_{\mathrm{pa}_r}(I \not \Phi R)} s_{\mathrm{pa}}(I \not \Phi d \not \Phi e^{-k_{\mathrm{pa}_r}(I \not \Phi R)} s_{\mathrm{pa}}(I \not \Phi d \not \Phi e^{-k_{\mathrm{pa}_r}(I \not \Phi R)} s_{\mathrm{pa}}(I \not \Phi d \not \Phi e^{-k_{\mathrm{pa}_r}(I \not \Phi R)} s_{\mathrm{pa}}(I \not \Phi d \not \Phi e^{-k_{\mathrm{pa}_r}(I \not \Phi R)} s_{\mathrm{pa}}(I \not \Phi d \not \Phi e^{-k_{\mathrm{pa}_r}(I \not \Phi R)} s_{\mathrm{pa}}(I \not \Phi d \not \Phi e^{-k_{\mathrm{pa}_r}(I \not \Phi R)} s_{\mathrm{pa}}(I \not \Phi d \not \Phi e^{-k_{\mathrm{pa}_r}(I \not \Phi R)} s_{\mathrm{pa}}(I \not \Phi d \not \Phi e^{-k_{\mathrm{pa}_r}(I \not \Phi R)} s_{\mathrm{pa}}(I \not \Phi d \not \Phi e^{-k_{\mathrm{pa}_r}(I \not \Phi R)} s_{\mathrm{pa}}(I \not \Phi d \not \Phi e^{-k_{\mathrm{pa}_r}(I \not \Phi R)} s_{\mathrm{pa}}(I \not \Phi d \not \Phi e^{-k_{\mathrm{pa}_r}(I \not \Phi R)} s_{\mathrm{pa}}(I \not \Phi d \not \Phi e^{-k_{\mathrm{pa}_r}(I \not \Phi R)} s_{\mathrm{pa}}(I \not \Phi d \not \Phi e^{-k_{\mathrm{pa}_r}(I \not \Phi R)} s_{\mathrm{pa}}(I \not \Phi d \not \Phi e^{-k_{\mathrm{pa}_r}(I \not \Phi R)} s_{\mathrm{pa}}(I \not \Phi d \not \Phi e^{-k_{\mathrm{pa}_r}(I \not \Phi R)} s_{\mathrm{pa}}(I \not \Phi d \not \Phi e^{-k_{\mathrm{pa}_r}(I \not \Phi R)} s_{\mathrm{pa}}(I \not \Phi d \not \Phi e^{-k_{\mathrm{pa}_r}(I \not \Phi R)} s_{\mathrm{pa}}(I \not \Phi e^{-k_{\mathrm{pa}_r}(I \not \Phi R)} s_{\mathrm{pa}}(I \not \Phi A \not \Phi e^{-k_{\mathrm{pa}_r}(I \not \Phi R)} s_{\mathrm{pa}}(I \not \Phi A \not \Phi e^{-k_{\mathrm{pa}_r}(I \not \Phi R)} s_{\mathrm{pa}}(I \not \Phi A \not \Phi e^{-k_{\mathrm{pa}_r}(I \not \Phi R)} s_{\mathrm{pa}}(I \not \Phi A \not \Phi e^{-k_{\mathrm{pa}_r}(I \not \Phi R)} s_{\mathrm{pa}}(I \not \Phi A \not \Phi e^{-k_{\mathrm{pa}_r}(I \not \Phi A \not \Phi A )} s_{\mathrm{pa}}(I \not \Phi A \not \Phi e^{-k_{\mathrm{pa}_r}(I \not \Phi A \not \Phi A )} s_{\mathrm{pa}}(I \not \Phi A \not \Phi A \not \Phi A \not \Phi A )$$

can be interpreted as the photon propagator of the mth band system. One should note that  $g_m(pR)$  depends on the density

of absorbing species constituting the gas, i.e.  $k_{pa}$ ,  $\mu$   $n_j$ , and therefore for the present problem is expressed as a function of gas pressure p times R, or in case of air as a function of partial pressure of  $O_2$ ,  $p_{O_2}$  times R (see section 3).

The equation (3) implies that the total photoionization rate is obtained via the summation of photoionization rates due to individual band systems. In problems concerned with photoionization due to multiple band systems, the evaluation of (3) may be time consuming. However, it may be possible to formulate quantities I(r,q) and g(pR) such that

$$\overset{M}{\overset{m}{\mathbf{a}}} I_m(r \overset{\mathbb{W}}{\phi} g_m(pR) = I(r \overset{\mathbb{W}}{\phi} g(pR)), \tag{5}$$

 $\mathring{\mathbf{a}} I_m(\overrightarrow{P} g_m(pR) = I(r \cancel{g} g(pR)),$  (5) where  $I(\overrightarrow{P} g)$  and g(pR) are referred to as intensity and photon propagator, respectively. In case (5) is satisfied, (3) reduces to

$$S_{\text{ph}_{i}}(\overrightarrow{r}) = \grave{Q}_{c} I(r \not \phi \frac{\cancel{R}(pR)}{4pR^{2}} dV \not c$$
 (6)

and the photoionization rate may be obtained by evaluating a single integral as opposed to M integrals.

#### 2.2. Differential formulation

Photoionization calculations in the form of (3) or (6) are time consuming due to the integral representation of the solution. However, following ideas in (Ségur et al 2006, Luque et al 2007, Bourdon et al 2007), one can formulate a computationally efficient model based on effective representation of the integral model by a set of Helmholtz differential equations. Here, the equation (6) will be used to demonstrate the approach. In principle, one can apply the same approach to each integral in (3) in case of photoionization problems where (5) is not satisfied. Having considered that g(pR) is generally a function of pR, the equation (6) can be rewritten in the form

$$S_{\text{ph}_{1}}(\overrightarrow{r}) = \grave{Q}_{\phi} I(r \phi \frac{\mathcal{P}_{1}g(pR)/(pR)}{4pR} dV \not c$$
 (7)

Considering the fact that

$$S_{\text{ph}_{1}}^{i}(\overrightarrow{r}) = \grave{Q}_{c}^{I}(r) (r) \frac{2 C_{i} e^{-l_{i}pR}}{4pR} dV \Leftrightarrow (8)$$

satisfies the Helmholtz differential equation (Bourdon et al 2007):

$$\mathbb{X}^{i}S_{\mathrm{ph}_{1}}^{i}(\stackrel{\square}{P}) - (l_{i}p)^{2}S_{\mathrm{ph}_{1}}^{i}(r) \stackrel{\square}{=} pC_{i}I(r) \qquad (9)$$

one can approximate g(pR)/(pR) in terms of a linear combination of exponential terms with fitting parameters  $C_i$  and  $l_i$ such that

$$\frac{g(pR)}{pR} \, \boxtimes \mathring{\mathbf{a}}_{i} \, C_{i} \mathbf{e}^{-l_{i}pR} \tag{10}$$

and consequently calculate the original  $S_{\mathrm{ph_{l}}}(\overrightarrow{r})$  via  $S_{\mathrm{ph_{l}}}(\overrightarrow{r}) = \mathring{\mathbf{a}} S_{\mathrm{ph_{l}}}^{i}(r) \stackrel{\boxed{\mathbb{M}}}{.}$ 

$$S_{\mathrm{ph}_{l}}(r) = \mathop{\mathsf{a}}_{i} S_{\mathrm{ph}_{l}}^{i}(r). \tag{11}$$

As a result, the solution for  $S_{ph_1}(r)$  may now be obtained by efficiently solving a set of Helmholtz differential equations of the form represented in (9). The number of differential

equations, which needs to be solved depends on the total number of exponents that provide a satisfactory fit to g(pR) in a specific range of pR values of interest. We note that one can use the partial pressure of an element in the gas (instead of p) in equations (7)–(10) For instance, in case of air, one can substitute p with  $p_{O_2}$  (see section 3.3).

#### 3. Photoionization of O<sub>2</sub> in air

#### 3.1. Photon propagator function

In case of photoionization of O<sub>2</sub> in air, equation (4) may be written in the form

$$g_m(pR) = \grave{Q}_{\phi} s_m(I \not \Phi \mathrm{e}^{-k_{\mathrm{pa}_{\mathrm{air}}}(I \not \Phi \mathcal{B})} \mathrm{pa}_{\mathrm{o}_2} I \times \mathcal{D}_{\mathrm{o}_2}^I(I) \not \Phi \ , \not \in (12)$$

where  $k_{\mathrm{pa}_{\mathrm{air}}} = k_{\mathrm{pa}_{\mathrm{O}_{2}}} + k_{\mathrm{pa}_{\mathrm{N}_{2}}}$ ,  $k_{\mathrm{pa}_{\mathrm{O}_{2}}}$ , and  $k_{\mathrm{pa}_{\mathrm{N}_{2}}}$  are the photo-absorption coefficients of air, O<sub>2</sub>, and N<sub>2</sub>, respectively. Generally, the aforementioned singlet states of N<sub>2</sub> in addition to NI and NII multiplets are the source of photons capable of ionizing O2 in air. However, the intensities of progressions from higher energy levels are dependent on the excitation mechanism of the molecule. Accordingly, multiple sources reporting N<sub>2</sub> XUV spectra were investigated. In particular, the spectra presented in Stephens et al (2016) is to the best knowledge of the authors, the only measured XUV spectra corresponding to an actual discharge in air. However, this spectra corresponds to the formative stage of a low temperature plasma. The authors characterize this stage in order to approximate the duration of the formation stage by assuming that an initial electron density  $n_0 = 10^3$  cm<sup>-3</sup> grows (via electron impact ionization with frequency  $n_i = 3$  ′  $10^8$  s<sup>-1</sup>) to the critical value  $n_{\rm crit} = 10^{18}$  cm<sup>-3</sup> after which the streamer initiates (see e.g. Pai et al 2010, and references therein). The ionization frequency corresponds to  $E \ \mathbb{M} E_k$  whereas the electric field in a streamer head is known to be a few factors larger than  $E_k$  and exists in a smaller volume and on shorter timescales than  $\sim$ 100 ns investigated in (Stephens *et al* 2016). Therefore, one would expect production of a different electron impact induced spectra due to streamer discharges in air. Additional time resolved measurements of the XUV spectra of a streamer discharge in air would be beneficial.

We also investigated spectra due to 100 eV (Heavs et al 2014) and 200 eV (Ajello et al 1989) electron impact excitation. As in the case of (Stephens et al 2016), multiplets of atomic nitrogen (i.e. NI and NII) contribute to these spectra, and the intensity of the bands changes as a function of the energy of the colliding electrons. Since for typical nonthermal discharge conditions the electron energy distribution function in air falls significantly for energies higher than 10 eV (e.g. Moss et al 2006), we do not consider these spectral data.

(Heavs et al 2014) also provide N<sub>2</sub> emission spectra due to 20 eV electron impact excitation. Similar to spectra resulting from 100 eV (Heavs et al 2014) and 200 eV (Ajello et al 1989) electron impact excitations, this spectra is recorded under optically thin conditions. As underscored by Stephens et al (2016), extension of such spectral data to

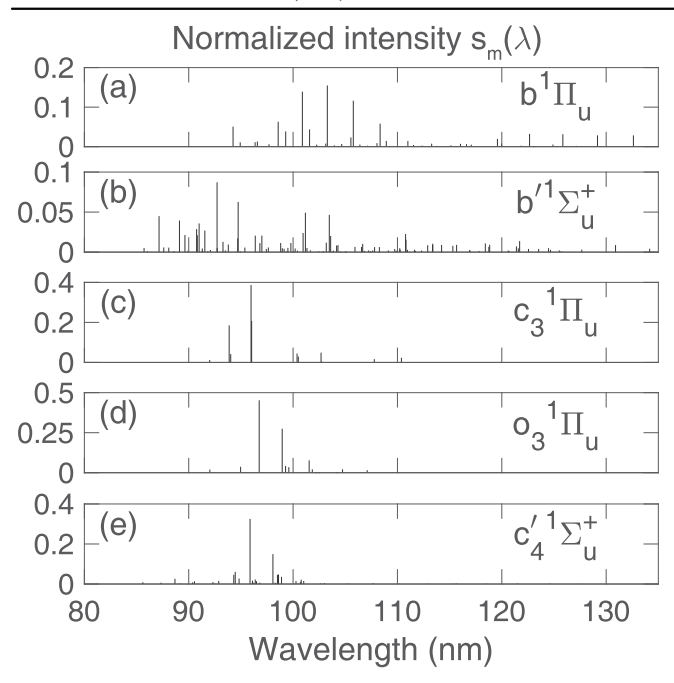


**Figure 1.** Normalized emission intensities for (a) Birge-Hopfield I, (b) Birge-Hopfield II, (c) Worley-Jenkins, (d) Worley, and (e) Carroll-Yoshino band systems generated during radiative transition from high energy singlet states of N<sub>2</sub> populated as a result of collisions with electrons with 20 eV energy. The data are deduced from the website accompanying (Heays *et al* 2014, Heays 2018, private communication).

high-pressure short-timescale scenarios resembling ground pressure conditions is questionable. Nevertheless, this is the only low-energy spectrum including emission bands due to radiative decay of all singlet states capable of emitting photons ionizing  $O_2$ . In the present work, we adopt this spectrum to study the individual contribution of Birge-Hopfield I, Birge-Hopfied II, Worley-Jenkins, Worley, and Carroll-Yoshino band systems of  $N_2$  to the photoionization of  $O_2$  for the first time. The adopted emission spectral data are depicted in figure 1. Note that there is no contribution from the NI and NII multiplets to this spectrum since 20 eV electron impact excitation cannot induce radiative transition of atomic multiplets as 20 eV lies below the threshold for N2 dissociation into excited N atoms with parity-allowed radiative decay channels (see e.g. Heavs et al 2014). Also, predissociation of N<sub>2</sub> after excitation to singlet states considered only produces N multiplets with very low excitation energies (see e.g. Walter et al 1994).

Note that spectra measured at low pressure may not be applicable to ground pressure conditions on long timescales considered in (Stephens *et al* 2016). Nevertheless, such spectra are valuable for modeling gas discharge phenomena at low air pressures (e.g. Pasko *et al* 2013, and references therein). In light of the discussion presented above, the authors believe that implementation of a fully time-dependent model which accounts for radiative transition, predissociation, collisional quenching, and electron impact excitation of various rovibrational levels of singlet states of  $N_2$  is necessary to synthesize the emission spectra of  $N_2$  under various conditions. Whereas radiative lifetimes and predissociation yields

have been determined for many of the rovibrational levels of these singlet states, to the best knowledge of the authors, there is essentially no studies with regards to the quenching of these levels. We note that majority of these singlet states have lifetimes of hundreds of picoseconds (see e.g. Sprengers 2006, and references therein) suggesting that the first few nanoseconds of the photoionization process may be significantly dynamic.

Additional details regarding the experimental setup for measuring the spectrum used here may be found in (Heays  $et\ al\ 2014$ ). Nevertheless, we note that the spectral data used here have been measured with a full width at half maximum (FWHM) of 0.2 Å (Heays  $et\ al\ 2014$ ). This is sufficiently high to resolve the rotational envelope profile of the  $N_2$  bands. We approximate each band by a Dirac delta function (see e.g. Dirac 1948, p 58) centered at the location of the band head. The emission spectrum of the mth band system may be written as

$$s_m(I) = \mathop{\mathsf{a}}_{n} a_{m,n} (I - I_{m,n}),$$
 (13)

where  $a_{m,n}$  is the intensity of the *n*th emission band of the *m*th band system and  $I_{m,n}$  is the location of the corresponding band head. Having substituted (13) into (12), we arrive at

$$g_m(p_{O_2}R) = a_{m,n}e^{-k_{air}(l_{m,n})R}s_{pa_{O_2}}(l_{m,n}) c_{O_2}(l_{m,n})$$
 (14)

for the photon propagator of the mth band system. To be consistent with previous formulations (e.g. Zheleznyak et al 1982, Naidis 2006) the implicit dependence of  $g_m(p_0, R)$  on the density of  $N_2$  and  $O_2$  is captured by  $p_{O_2}$ , considering air as a 20%  $O_2$ , 80%  $N_2$  mixture. We note that the data compilations of Fennelly and Torr (1992) for the photoabsorption cross sections of N2 and O2, and the photoionization yield of O2 have been used to calculate (14) for the aforementioned singlet states. Figure 2 depicts  $g_m(p_{O_2}R)/(p_{O_2}R)$  for each of the singlet states. The photon propagator is a quantitative measure of O2 photoionization events at a certain  $p_{O_2}R$  value. For instance, it is inferred from figure 2 that at constant pressure, photons of the Worley band system (i.e. emitted from the  $o_3^1 P_u$  state) are most capable of photoionizing O2 at both short and long distances. On the other hand, compared to photons emanating from other singlet states, photons of the Birge-Hopfield I band system (i.e. generated by the  $b^1 P_u$  state) are least capable of photoionizing  $O_2$  at short distances.

#### 3.2. Source of radiation

In order to employ the photoionization framework introduced in section 2, we need to quantify the source of emission for each band system. The intensity of radiation from each singlet state may be defined via  $I_m = A_m n_m$  where  $A_m$  is the Einstein coefficient, i.e. spontaneous emission frequency for state m. The density of the excited state,  $n_m$  can be calculated using a fully time-dependent model (Sipler and Biondi 1972):

$$\frac{\P n_m}{\P t} = -\frac{n_m}{t_m} + \underset{m \notin}{\mathring{a}} A_{m \notin n_m t_{\notin}} n_m^{\mathbb{M}} n_e, \qquad (15)$$

where the sum over the terms  $A_{m} \not\in n_m$  represents increase in  $n_m$  due to cascading from higher energy states,  $\tau_m$  denotes the

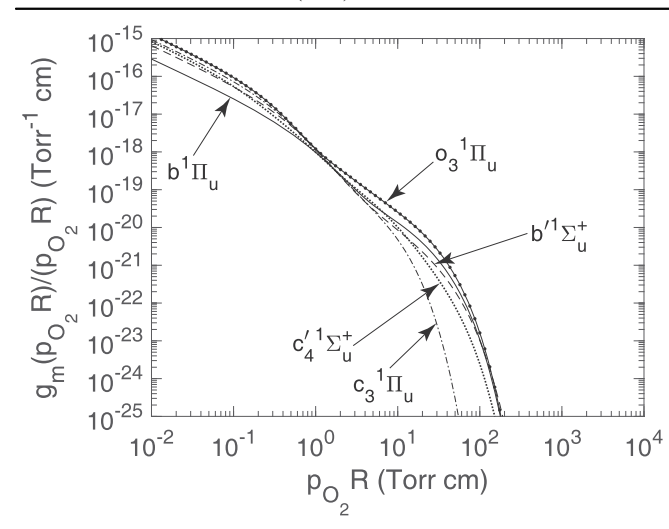


**Figure 2.** The function  $g_m(p_{O_2}R)/(p_{O_2}R)$  for  $b^1P_u$ ,  $b \not\in S_u^+$ ,  $c_3^1P_u$ ,  $o_3^1P_u$ ,  $c \not\in S_u^+$  states of  $N_2$ .

total lifetime of state m including effects of collisional quenching, predissociation, and spontaneous emission,  $n_m^{\mathbb{N}}$  is the excitation frequency of state m due to electron impact, and  $n_e$  denotes electron density. We solve (15) under steady state conditions due to the extremely short lifetime of singlet states (e.g. Sprengers 2006, and references therein) and negligible cascading from higher energy states (e.g. Malone  $et\ al\ 2012$ ). Furthermore, we neglect effects of predissociation in spite of the fact that some rovibrational levels of these singlet states are heavily predissociated (see e.g. Heays 2011, and references therein). This is mainly due to the lack of a comprehensive model which considers each rovibrational level of an electronic state individually. Developing such a model is out of the scope of the present work. As a result, and following notation in the previous literature we arrive at

$$I_m = A_m t_m n_m^{\text{M}} n_e = \frac{p_q}{p + p_q} n_m^{\text{M}} n_e, \qquad (16)$$

where we utilized the fact that  $\tau_m$  is reduced compared to the lifetime in the absence of quenching, predissociation, and cascading,  $A_m^{-1}$ , by the factor  $Q = p_q/(p + p_q)$  where  $p_q = 30$  Torr, denotes the quenching pressure for all singlets states and corresponds to air pressure at 24 km altitude in the Earth's atmosphere (e.g. Naidis 2006, Pancheshnyi 2015).

In order to calculate the excitation frequency of the singlet states, we input the electron impact excitation cross section of these states (Itikawa 2006) to BOLSIG+ software (Hagelaar and Pitchford 2005) and calculate the excitation frequency for each state as a function of the reduced electric field E/N, where N denotes the neutral atmospheric density. In particular, we use two separate sets of cross sections. In the first case, we use cross sections from (Malone *et al* 2012), where each of the singlet states has it is own set of electron impact excitation cross sections and respective excitation threshold energies of  $b^1P_u$  (12.49 eV),  $b_s^dS_u^+$  (12.85 eV),  $c_3^1P_u$  (12.91 eV),  $o_3^1P_u$  (13.10 eV),  $c_s^dS_u^+$  (12.93 eV) (Khakoo *et al* 2008). As a result, we calculate the excitation frequency of individual singlet states,  $n_m^{[M]}$  In addition, we obtain

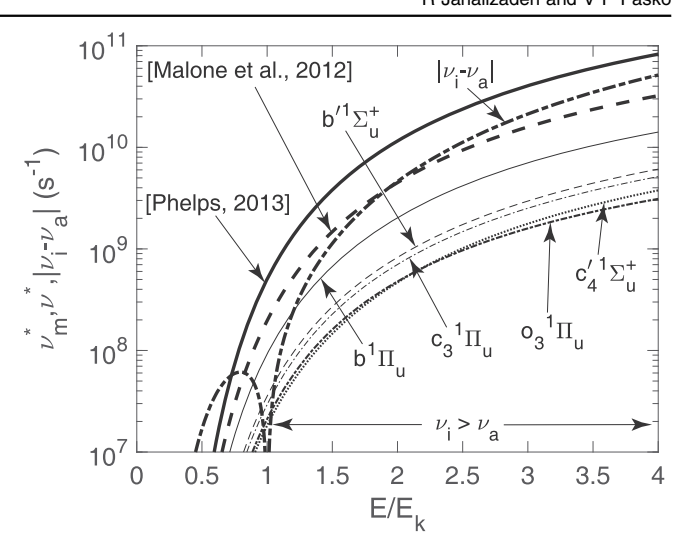


**Figure 3.** Excitation frequencies for  $b^1P_u$ ,  $b\not \in S_u^+$ ,  $c_3^1P_u$ ,  $o_3^1P_u$ ,  $c\not \notin S_u^+$  states of  $N_2$ , total excitation frequency of singlet states,  $n^{[m]}$  in case of cross sections from (Malone *et al* 2012) and (Phelps 2013), and effective electron impact ionization frequency  $|n_i - n_i|$ 

the total excitation frequency of all singlet states denoted hereafter by  $n^{\text{t}}$  where  $n^{\text{t}}$  a  $_{m=1}^{M} n_{m}^{\text{t}}$ .

The second set of cross sections is due to Phelps (2013) (see Pancheshnyi et al 2012 and web link therein) and is labeled sum of singlet states in the database. The cross sections provided in this database are the aggregate cross section of all singlet states with a single excitation threshold of 13 eV. As a result, in this case one can only calculate  $n^{\square}$  and therefore,  $I_m(r)$  may not be defined. Nevertheless, as demonstrated in (e.g. Liu and Pasko 2004), an emission intensity and a photon propagator (similar to (5)) are defined in order to calculate the photoionization rate. The corresponding excitation frequencies for each singlet state are depicted in figure 3 in which  $E_k = 32 \text{ kV cm}^{-1}$  denotes the reference magnitude of the breakdown electric field at ground air pressure. In addition, the total excitation frequency of singlet states due to cross sections from Phelps (2013) and Malone et al (2012) are presented in the same figure. We also include the effective ionization frequency  $|n_i - n_i|$  where  $\nu_i$ and  $n_a$  denote electron impact ionization frequency and two body dissociative attachment frequency, respectively. As will be further discussed in the following sections and appendix B, the ratio  $n^{\mathbb{N}} n_i$  is an important quantity on which the photoionization efficiency of a medium depends on.

#### 3.3. Total photoionization rate and fit development

At this point, the rate of  $O_2$  photoionization in air can be obtained using the integral formulation (3). However, we wish to find the emission intensity and the photon propagator for which equation (5) is satisfied. In that case, photoionization rate calculations reduce to evaluating (6). We express  $I(r_0^{(k)})$  in terms of the intensity of emissions produced by all singlet states of  $N_2$ . The quantity  $I(r_0^{(k)})$  represents the total number of photons emitted per unit volume per unit time due

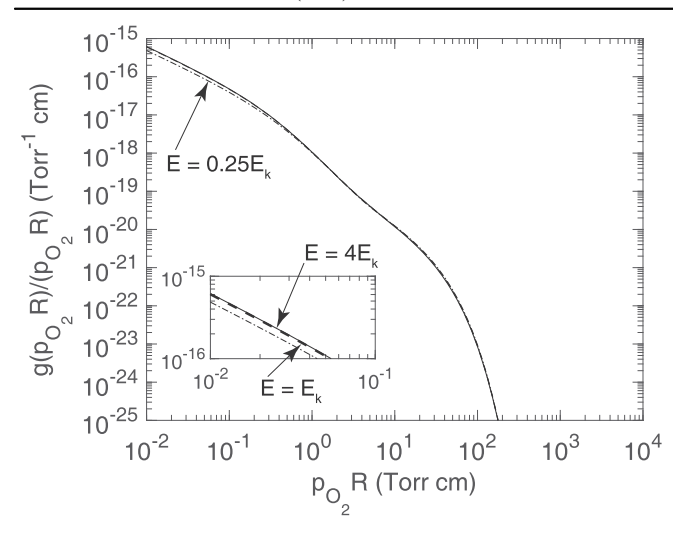


**Figure 4.** The function  $g(p_{O_2}R)/(p_{O_2}R)$  for  $E = 0.25E_k$ ,  $E = E_k$ , and  $E = 4E_k$ .

to radiative decay of all states considered, and therefore

$$I(r \phi) = \mathring{\mathbf{a}}_{m}^{M} I_{m}(r \phi) = \frac{p_{q}}{p + p_{q}} n \mathcal{A}_{e}(r \phi). \tag{17}$$

Once  $I(\overrightarrow{r}, \overrightarrow{q})$  is determined, using (5), (16), and (17) we arrive at

$$g(\boldsymbol{n}_{m}^{\mathbb{X}}, \boldsymbol{p}_{\mathcal{O}_{2}}R) = \frac{1}{\boldsymbol{n}^{\mathbb{X}}} \overset{M}{\underset{m=1}{\overset{M}{\overset{M}{\otimes}}}} \boldsymbol{n}^{\mathbb{X}}_{m} \boldsymbol{g}_{m}(\boldsymbol{p}_{\mathcal{O}_{2}}R). \tag{18}$$

The equation (18) demonstrates that in addition to  $p_{Q_2}R$ , the photon propagator is now also a function of  $n_m^{\mathbb{N}}$  and has dependence on the reduced electric field. Figure 4 depicts  $g(n_m^{\mathbb{N}}, p_{Q_2}R)$  for three representative cases of  $E = 0.25E_k$ ,  $E = E_k$ , and  $E = 4E_k$ . It can be seen from this analysis that the variation of  $g(n_m^{\mathbb{N}}, p_{Q_2}R)$  as a function of the applied reduced electric field is negligible and photon propagators corresponding to different applied fields are essentially the same. Therefore, one can assume a single photon propagator,  $g(p_{Q_2}R)$ , to solve the problem of photoionization of  $Q_2$  in air. In the rest of the present work, we adopt  $g(p_{Q_2}R)$  corresponding to  $E = E_k$ .

Table 1 provides the parameters for a 6-exponent fit to the photon propagator depicted in figure 4. Using these parameters, one can obtain the solution to the problem of O<sub>2</sub> photoionization via a set of equivalent Helmholtz differential equations, and consequently, calculate the photoionization rate efficiently. As pointed out in section 2.2, we express the fit in terms of  $p_{O_2}$  (i.e. substitute p with  $p_{O_2}$  in equations (7)– (10). This is solely done to be consistent with previous works (e.g. Zheleznyak et al 1982, Naidis 2006, Pancheshnyi 2015), where results have been published as a function of both pRand  $p_{\Omega}$ , R. The introduced 6-exponent fit to  $g(p_{\Omega}, R)/(p_{\Omega}, R)$ is compared with the calculated photon propagator in figure 5. As demonstrated in this figure, the fit follows the calculated function with high accuracy in a wide range of  $p_{O_2}R$  values. The photon propagator in case of no absorption by  $N_2$  and  $O_2$ (i.e. reflecting simple geometrical spreading of photons ~  $1/(4pR^2)$ ) is also depicted for comparison. As expected

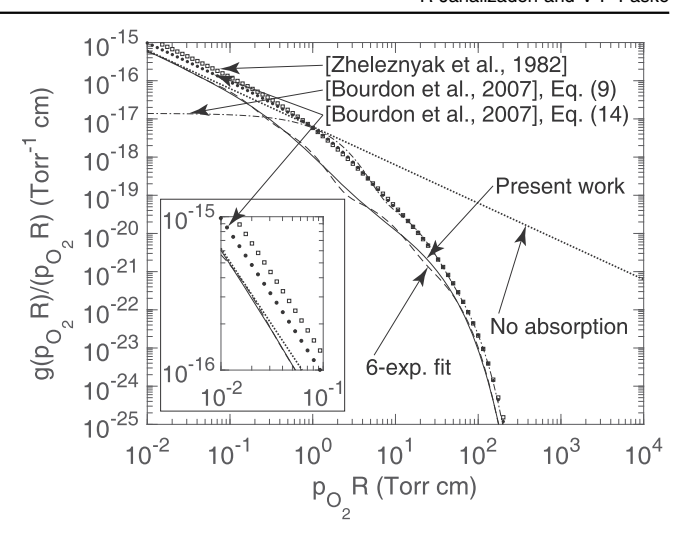


**Figure 5.** Comparison of  $g(p_{O_2}R)$  with  $g^Z(p_{O_2}R)$ , i.e. the photon propagator of (Zheleznyak *et al* 1982) (see equation (A.8)). In addition, the 6-exponent fit to  $g(p_{O_2}R)/(p_{O_2}R)$  and the 3-exponent fits to  $g^Z(p_{O_2}R)/(p_{O_2}R)$  introduced in (Bourdon *et al* 2007) are depicted.

**Table 1.** Parameters for the fit  $\frac{g(p_{O_2}R)}{(p_{O_2}R)}$  Må  $_iC_i\mathrm{e}^{-l_ip_{O_2}R}$ .

j	$C_j$ (cm Torr <sup>-1</sup> )	$l_j (\text{cm}^{-1} \text{Torr}^{-1})$
1 2 3	9.850 5(-16) <sup>1</sup> 1.751 8(-16) 1.393 3(-17)	90.331 5 14.678 4 2.529 3
4 5 6	1.505 8(-19) 5.320 0(-21) 1.862 3(-23)	0.265 2 0.062 7 0.041 0

<sup>&</sup>lt;sup>1</sup> Read  $9.8505 \times 10^{-16}$ .

effects of absorption become negligible for small  $p_{O_2}R$  values.

As already mentioned in (Bourdon et al 2007), in order to calculate the rate of photoionization, it suffices to know the isotropic part of the photon distribution function,  $F_0(F)$ . We note that equation (6) of (Ségur et al 2006) arrives at the same conclusion. As illustrated in (Ségur et al 2006), equation (12),  $F_0(f)$  is expressed as a linear combination of  $F_{0,j}(f)$ , where  $F_{0,j}(f)$  denotes the isotropic part of the photon distribution function  $F_j(f)$ , satisfying the monochromatic radiative transfer equation (see equation (10) in (Bourdon et al 2007)). We note that  $\mathsf{F}_{\mathrm{SP}_3,0,j}(F)$  is expressed as a linear combination of functions  $I_{1,j}$  and  $\varphi_{2,j}$  which respectively satisfy equations (18) and (19) of (Bourdon et al 2007). Hence, for  $j = 1, ..., N_g, 2 \times N_g$  equations need to be solved where  $N_g$  is the number of effective monochromatic radiative transfer equations. In the SP<sub>3</sub> model,  $N_g = 3$ , and therefore, a set of six differential equations should be solved to calculate the photoionization rate, which is equivalent to the 6-exponent fit proposed in this work. Also note that the number of fits represents a trade-off between accuracy and number of differential equations to solve. Lower number of fits were also tried. However, 6 terms provided sufficient accuracy for the

full range  $10^{-2} < p_{\rm O_2}R < 10^4$  Torr cm considered in this work.

#### 4. Results and discussion

#### 4.1. Comparison with (Zheleznyak et al 1982)

Currently, the most widely used model for photoionization calculations in air is due to Zheleznyak et al (1982). The satisfactory agreement of the model with previous photoionization measurements in air (e.g. Teich 1967, Penney and Hummert 1970, Aints et al 2008) has been demonstrated and extensively discussed (see e.g. Naidis 2006, Aints et al 2008, Pancheshnyi 2015). Nevertheless, there have been a number of approximations employed in the development of the model. In particular, the photoabsorption cross section of O<sub>2</sub> in the 98–102.5 nm interval is approximated by an analytical function (Mnatsakanyan and Naidis 1991), which does not capture the complex behavior of the photoabsorption cross section of O<sub>2</sub> represented in measurements (e.g Fennelly and Torr 1992, Keller-Rudek et al 2013). The same applies to the photoionization yield of O<sub>2</sub>. Furthermore, it is assumed that radiation with wavelengths shorter than 98 nm is exclusively absorbed by N2 and therefore has no contribution to the photoionization of  $O_2$ . We note that although photoabsorption cross sections of N2 and O2 are considerably high below 98 nm, it is necessary to account for the complexity of the photabsorption cross sections of the two species in addition to the wavelength resolved emission spectra of excited N<sub>2</sub> singlet states (Ajello et al 1989, Heays et al 2014).

The additional difficulty is related to the quantification of the source of photoionizing radiation. The excitation frequency of singlet states responsible for photoionizing emission from N<sub>2</sub>, tabulated in (Zheleznyak *et al* 1982), is an approximation in an effort to fit photoionization rate calculations to experimental results. As demonstrated in the previous sections, the issues mentioned above have been addressed in the new model. In particular, we considered the entire XUV emission spectrum of N<sub>2</sub>, used experimental values for the photoionization cross sections of N<sub>2</sub> and O<sub>2</sub> along with the photoionization yield of O<sub>2</sub>, and calculated the excitation frequency of the singlet states of N<sub>2</sub> using recently measured electron impact excitation cross sections.

A detailed derivation of the model of Zheleznyak *et al* (1982) in terms of the general photoionization framework is provided in appendix A for further reference. Since both the model introduced in the present work and the model of Zheleznyak *et al* (1982) reduce to the same integral representation given by equation (6), we compare them by highlighting the differences between the intensity and photon propagator functions calculated by the two models. Figure 5 compares the photon propagator calculated in this work with the photon propagator derived from the model of Zheleznyak *et al* (1982),  $g^Z(p_{O_2}R)$ , calculated in equation (A.8). It is observed that  $g^Z(p_{O_2}R)$  is generally greater than the photon propagator introduced here, and both functions have similar

**Table 2.** Ratio of excitation frequency of singlet states to ionization frequency,  $\overline{x_{0_2}} n^{[x]} n_i$  obtained using cross sections of (Malone *et al* 2012) and (Phelps 2013) compared to the model of Zheleznyak *et al* (1982). See text for further details.

E/p (V cm <sup>-1</sup> Torr <sup>-1</sup> )	(Zheleznyak et al 1982)	(Malone et al 2012)	(Phelps 2013)
30	0.05	1.10	2.69
50	0.12	0.87	2.26
100	0.08	0.59	1.50
200	0.06	0.39	1.02

behavior as a function of  $p_{O_2}R$ . In addition, the exponential fits developed in (Bourdon *et al* 2007) with the purpose of converting the integral representation of the model of Zheleznyak *et al* (1982) to a set of Helmholtz differential equations are also shown in figure 5. It is inferred that the 6-exponent fit introduced in the present work follows the corresponding photon propagator more accurately, especially for lower values of  $p_{O_2}R$ . The fitting functions introduced by equations (9) and (14) of (Bourdon *et al* 2007) were defined in the range  $1 < p_{O_2}R < 150$  and  $0.1 < p_{O_2}R < 150$  Torr cm, respectively. The 6-exponent fit with parameters in table 1 is designed for the range  $10^{-2} < p_{O_2}R < 10^4$  Torr cm and therefore, may be applied to problems with a greater range of  $p_{O_2}R$  variations.

Having compared equations (17) and (A.5) one concludes that the total excitation frequency of the singlet states of N<sub>2</sub> is the main factor which may cause difference in the photoionizing source (i.e. intensity) calculated by the present work and the model of (Zheleznyak et al 1982). We note that  $p_{\rm q}=30$  Torr in both models and that the average photoionization yield of  $O_2$ ,  $\overline{X_{O_2}^Z}$ , present in (A.5) is a scaling factor close to one and therefore, does not contribute extensively to the intensity in the model of Zheleznyak et al (1982),  $I^{Z}(P_{\phi})$ . While  $n^{\square}$  has been directly calculated in the present work (see figure 3), the model of Zheleznyak et al (1982) provides numerical values for the ratio  $\overline{X_{O_2}} n^{\text{N}} n_i$  at certain E/pvalues. In order to compare our results with those cited by Zheleznyak et al (1982), we calculate  $\overline{x_{0}}_{n} n^{\text{T}} n_{i}$  at the same E/p values. Having considered the distribution of  $X_{O_2}(I)$ presented in figure A1(a), we approximate the average photoionization yield of  $O_2$  as  $\overline{X}_{O_2}$  [ $\underline{W}$ ]0.7. Table 2 presents the calculated results. It can be seen that the ratios obtained using cross sections from (Malone et al 2012) and (Phelps 2013) are both generally greater, and for some E/p values exceed the Zheleznyak et al (1982) model values,  $\overline{x_{0}^{Z}} n^{[x]}/n_i$ , by an order of magnitude. In addition, the peak for  $\overline{x_{\mathrm{O}_2}^{\mathbb{Z}}} n^{\underline{\mathbb{W}}} / n_i$  occurs at a different location from  $\overline{X_{0}}_{n} n^{[n]} n_{i}$ . For cross sections from (Malone et al 2012) and (Phelps 2013), the peak value is located at  $E/p = 23.5 \text{ V cm}^{-1} \text{ Torr}^{-1}$  and  $E/p = 28.5 \text{ V cm}^{-1} \text{ Torr}^{-1}$ , respectively. The general behavior of  $\overline{x_{0}}$ ,  $n^{[\underline{w}]}/n_i$  however, is the same for both the present work and the model of Zheleznyak et al (1982). These results are not shown here for the sake of brevity.

## 4.2. O<sub>2</sub> photoionization rate calculations for short and long ranges

The possibility of large-scale gas discharge events above thunderclouds, which we currently know as sprite phenomenon (e.g. Stenbaek-Nielsen et al 2013, Pasko et al 2013, and references therein) was first predicted in 1925 by the Nobel Prize winner C.T.R. Wilson (Wilson 1925), and first documented in 1989 by Franz et al (1990). Observation of such events occurring at lower ionospheric altitudes underscores the importance of accurately modeling photoionization in air at low air pressures at high altitudes. The length scale on which photoionization occurs is highly dependent on air pressure. As we go to higher altitudes in Earth's atmosphere, air density drops exponentially. Therefore, a photon at high altitudes encounters fewer molecules along its path and travels a much longer distance before getting absorbed by the molecules in air. The same conclusion can be derived from table 1 where the photoabsorption coefficient terms  $l_i p_{O_2}$  drop exponentially as a function of altitude. The model of Zheleznyak et al (1982) provides a straightforward quantitative approach for calculating the maximum range at which photoionization is considerable in a certain problem. Assuming that only the term with  $\chi_{min}$  (see appendix A) governs the long range behavior of the photon propagator, one concludes that at ground pressure, an e-fold reduction in  $g^{\mathbb{Z}}(p_{\Omega_n}R)$ occurs at a distance  $R \simeq 2 \,\mathrm{mm}$  while at 80 km altitude, the same reduction happens for  $R \simeq 125 \,\mathrm{m}$ . In addition to discussing the dynamics of the photoionization scale as a function of altitude, it is necessary to consider the effect of altitude variation on the source of radiation. Quenching of XUV photons is negligible at high altitudes since the quenching factor Q approaches one as p decreases to values  $p \ll p_q$ . As a result, the relative number (i.e. scaled with similarity laws (Liu and Pasko 2004)) of generated XUV photons is enhanced at higher altitudes.

Exploring the effect of quenching factor, air density, and photoionization scale on an electric discharge is an interesting problem. Due to the interplay of such effects, the characteristics of a discharge at high altitudes are significantly modified compared to those at ground pressure (see e.g. Qin and Pasko 2015). In this section we provide quantitative results demonstrating the performance of the new model using simple representative sources. In particular, we emphasize practical employment of this model at different pressure conditions and different distances from the source for two representative cases that we are referring to as: (i) short range and (ii) long range. In particular, scenario (i) is introduced to calculate the photoionization rate of  $O_2$  due to a large radiator resembling the sprite halo (see e.g. Barrington-Leigh et al 2001, Frey et al 2007) whereas scenario (ii), is introduced to calculate the photoionization rate of O2 due to a small radiator with characteristics similar to a sprite streamer (see e.g. McHarg et al 2007, Stenbaek-Nielsen et al 2013). The source of radiation in both cases is a sphere emitting photons at a constant rate per unit volume per unit time in an axisymmetric simulation domain defined using conventional cylindrical coordinates  $(\rho, \phi, z)$ . The size of the simulation domain is characterized by the respective radial and vertical dimensions  $l_o$  and  $l_z$ , and the simulation is performed at air pressure corresponding to altitude  $h_0 = 80$  km in the Earth's atmosphere. That is the lower edge of the domain is located at 80 km and the center of the sphere is located at  $(r_0, z_0) = (0, h_0 + l_z/2)$ . We assume constant pressure in the simulation domain equal to  $p(h_0) = 0.0114$  Torr, which corresponds to O<sub>2</sub> density  $n_{\rm O_2} = 8$  ′  $10^{19}$  m<sup>-3</sup>. To maintain connection to previous work, we adopt the model of Morrow and Lowke (1997) to calculate  $\nu_i$  and  $\nu_a$ . The differences between  $\nu_i$  and  $\nu_a$  models introduced in (Morrow and Lowke 1997) and those calculated from (Phelps 2013) set of cross sections using BOLSIG+ are small and do not affect any conclusions of the present work. In addition, we use  $n^{[k]}$ calculated from inputting the cross sections of Malone et al (2012) to BOLSIG+ in order to quantify the source of radiation for the present work.

- (i) Long range: In this case the radius of the sphere is  $a=2.5\,\mathrm{km}$  and the size of the simulation domain is  $(l_p,l_z)=(10,10)\,\mathrm{km}$ . In addition,  $E/N=117\,\mathrm{Td}$  (1 Td =  $10^{-21}\,\mathrm{V}$  m<sup>2</sup>,  $E=47.3\,\mathrm{V}$  m<sup>-1</sup> and  $N=4\times10^{20}$  m<sup>-3</sup>) and  $n_\mathrm{e}=4.5\,\mathrm{'}$  10<sup>8</sup> m<sup>-3</sup> in the source region and zero elsewhere. As a result, emission intensity values for the present work and the model of Zheleznyak *et al* (1982) are  $I=1.25\times10^{12}\,\mathrm{m}^{-3}\,\mathrm{s}^{-1}$  and  $I^Z=1.24\,\mathrm{'}$  10<sup>11</sup> m<sup>-3</sup> s<sup>-1</sup>, respectively.
- 10<sup>11</sup> m<sup>-3</sup> s<sup>-1</sup>, respectively.

  (ii) Short range: In this case the radius of the sphere is a = 50 m and the size of the simulation domain is  $(l_{\rho}, l_{z}) = (1,1)$  km. In addition, E/N = 320 Td  $(E = 129 \text{ V m}^{-1} \text{ and } N = 4 \times 10^{20} \text{ m}^{-3})$  and  $n_{\rm e} = 4.5$  ′  $10^{10}$  m<sup>-3</sup> in the source region and zero elsewhere. As a result, the emission intensity values for the present work and the model of Zheleznyak *et al* (1982) are  $I = 8 \times 10^{15}$  m<sup>-3</sup> s<sup>-1</sup> and  $I^{Z} = 8.99 \times 10^{14}$  m<sup>-3</sup> s<sup>-1</sup>, respectively.

Figures 6(a) and (b) depict photoionization results for the new model in case of the long and short range problems, respectively. Additionally, we have included results from the model of Zheleznyak *et al* (1982) in which case we linearly interpolate the data provided in table 2 to quantify the source for a certain E/N. In the following, the calculation method corresponding to each label in figures 6(a) and (b) is defined as:

- First principles: We use the intensity and the photon propagator of the new model respectively defined in (17) and (18), and the integral representation is used for the entire simulation domain.
- 6-exp. int.: Intensity is defined in (17) and the photon propagator is approximated by the 6-exponent fit with parameters in table 1. The solution is obtained using the integral representation in the entire simulation domain.
- 6-exp. diff.: Intensity is defined in (17) and the photon propagator is approximated by the 6-exponent fit with parameters in table 1. The integral representation is used for the boundaries only, whereas (9) is solved for the interior points. Note that  $p_{\rm O_2}$  substitutes p in (9).
- (Zheleznyak *et al* 1982): The intensity and photon propagator of the model of Zheleznyak *et al* (1982) are

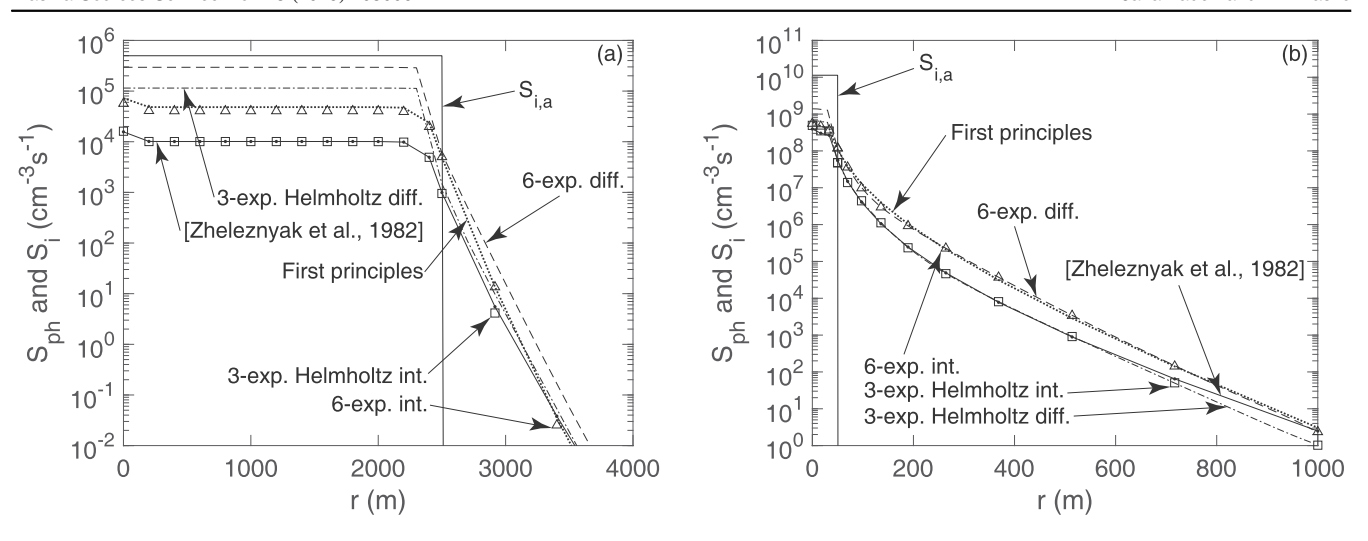


**Figure 6.** Radial scans  $S_{\rm ph}(r, z_0)$  for (a) the long range and (b) short range problem.

provided in (A.5) and (A.8), respectively. The integral representation is used for the entire simulation domain.

- 3-exp. Helmholtz int.: Intensity is defined in (A.5) and the photon propagator defined in (A.8) is approximated with the 3-exponent Helmholtz fit with parameters in (Bourdon *et al* 2007). The integral representation is used for the entire simulation domain.
- 3-exp. Helmholtz diff.: Intensity is defined in (A.5) and the photon propagator defined in (A.8) is approximated with the 3-exponent Helmholtz fit with parameters in (Bourdon *et al* 2007). The integral representation is used for the boundaries only, whereas (9) is solved for the interior points with fit parameters from (Bourdon *et al* 2007). Note that  $p_{O_2}$  substitutes p in (9).

The boundary value for solutions obtained via the differential representation are calculated in integral form using the corresponding fit to the photon propagator. It is assumed that only the term with the lowest photoabsorption coefficient contributes to photoionization at the boundary and therefore, the calculated boundary values are assigned to this term. The contributions from other terms are set to zero. As a result, the photoionization rate on the boundaries, obtained from the summation of individual terms, equals the photoionization rate calculated using the integral form.

From figures 6(a) and (b) it is inferred that the photoionization rate calculated by the new model is generally higher than that from the model of Zheleznyak *et al* (1982) by a factor of 2 to 3. Nevertheless, as will be demonstrated in the next section, the two models give similar results while simulating streamers, indicating quantitative consistency of the models. In particular, figure 6(b) roughly approximates the parameters of a streamer head at ambient air pressure corresponding to 80 km altitude. It is seen that in this case, the net ionization source  $S_{i,a} = (n_i - n_a)n_e$  dominates photoionization in the source region (streamer head). We note that the dynamics of a streamer is essentially governed by the streamer head(s). Therefore, one may argue that photoionization deviations of the two models may not affect the discharge properties significantly.

#### 4.3. Double-headed streamer in air

In this section, we report and compare modeling results on a double-headed streamer developing in air at ground pressure by solving the convection-diffusion equations, i.e. plasma fluid model equations, for electrons and ions coupled with Poisson's equation in an axisymmetric cylindrical domain (see e.g. Dhali and Williams 1987, Vitello et al 1994, Kulikovsky 1997). We consider three separate cases where: (i) we adopt the photoionization model of Zheleznyak et al (1982) and use plasma fluid model coefficients of Morrow and Lowke (1997), (ii) we implement the photoionization model introduced in the present work and utilize plasma fluid model coefficients defined in (Morrow and Lowke 1997), and finally (iii) we implement the photoionization model of the present work and input cross sections from (Phelps 2013) to BOLSIG+ to calculate plasma fluid model coefficients. In all cases the photoionization rate of O2 is calculated using the fits to the corresponding photoionization model. That is, the 3-exponent Helmholtz fit of Bourdon et al (2007) to the photoionization model of Zheleznyak et al (1982) and the 6-exponent fit to the photoionization model developed in the present work are implemented in respective cases. Furthermore, differential representations of the fits are employed to perform photoionization calculations for the interior points of the simulation domain while integral representation of the fits are used to update boundary values.

We solve the transport equations for the charged species implementing the second order piecewise linear flux-limiting technique (Mignone 2014) and solve Poisson's equation for potential using the successive over-relaxation (SOR) method with a previously assigned accuracy limit of  $\epsilon=10^{-10}$  as the convergence criterion (see e.g. Hockney and Eastwood 1988, p 179). The solution to the Hemholtz differential equations for photoionization have also been obtained via the SOR method. First order time-stepping is achieved using the Forward Euler (FE) method (Potter 1973, p 27). Note that Bagheri *et al* (2018) provide a survey of a set of codes used for simulating streamers in air which may be considered as benchmarks to which one can compare the performance of a self-implemented code.

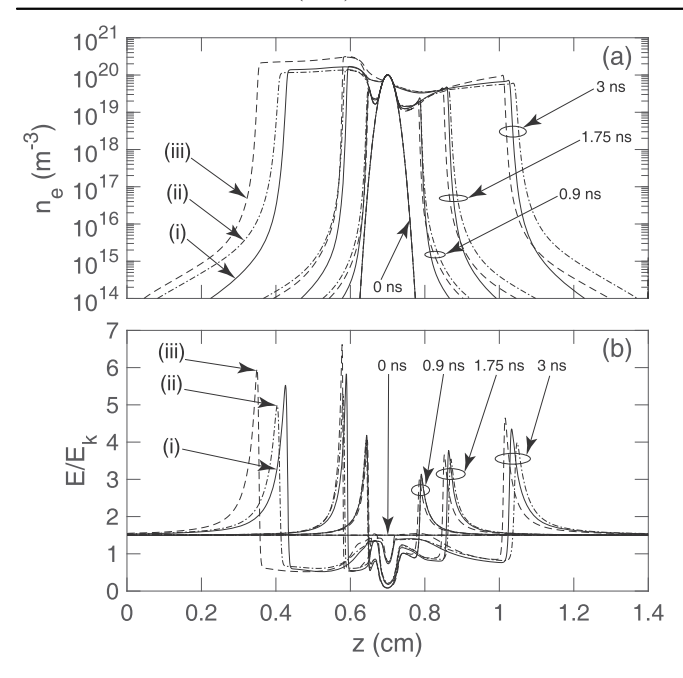


**Figure 7.** Axial scan of (a) electron density and (b)  $E/E_k$  for  $t_0 = 0$  ns,  $t_1 = 0.9$  ns,  $t_2 = 1.75$  ns, and  $t_3 = 3$  ns for cases (i), (ii), and (iii) defined in section 4.3.

We note that case (i) corresponds to the streamer simulated in (Bourdon et al 2007). Therefore, we adopt the exact simulation geometry and parameters described in (Bourdon et al 2007) for all three cases in order to compare the effect of various models for photoionization and plasma fluid coefficients on the streamer properties. Figures 7(a) and (b), respectively, depict the axial scan of electron density and electric field as a function of time for all three cases up until t=3 ns. In parituclar, figure 7(a) corresponds to figures 9 and 10(a) in (Bourdon et al 2007) while figure 7(b) corresponds to figure 10(b) in (Bourdon et al 2007). Upon comparison, one can see satisfactory agreement between results for case (i) and those published in (Bourdon et al 2007). In addition, figure 8 depicts cross-sectional views of the electron density at t = 3.5 ns for streamers simulated in the aforementioned three cases. From figures 7 and 8 it is inferred that the effect of models governing the plasma fluid coefficients on the streamer dynamics is much more pronounced compared to the contribution of the photoionization models. This can be inferred from the similarity of the results for cases (i) and (ii), where only the photoionization model has been changed. In particular, electron density values are similar for the two cases in the streamer head region, where electron impact ionization dominates photoionization. The two cases diverge at regions ahead of the streamer where photoionization is the main contributor to the electron-ion pair production. From figure 7(a) it is inferred that photons modeled in the present work travel longer distances as the electron density for cases (ii) and (iii) is higher at farther locations ahead of the streamer head compared to case (i). There is a considerable difference between the first two cases and case (iii) in the streamer head. This may be due to deviations of  $n_a$ values calculated in cases (ii) and (iii). The divergence is most

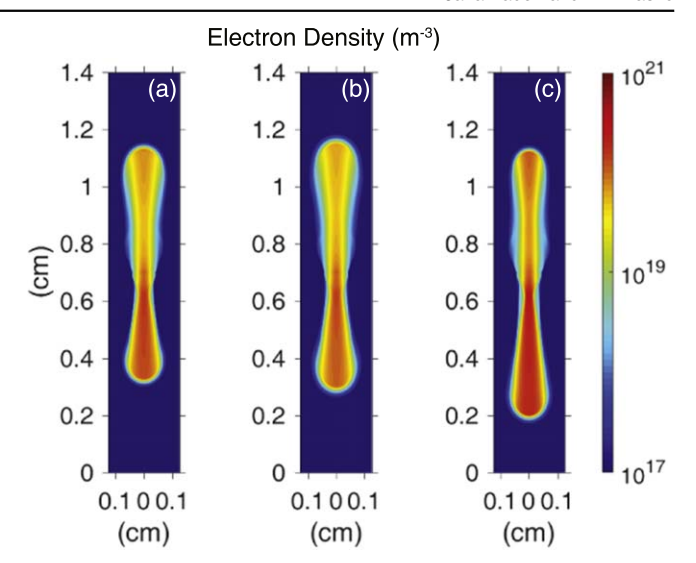


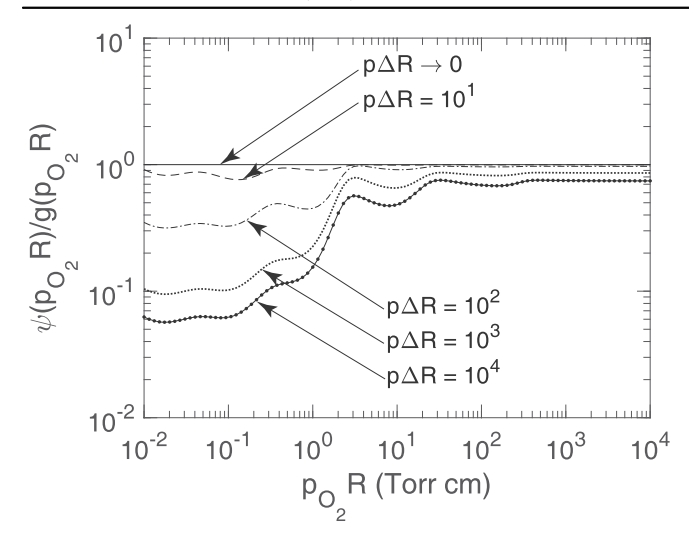
**Figure 8.** Cross-sectional view of electron density distribution at t=3.5 ns for (a) case (i), i.e. streamer in (Bourdon *et al* 2007), (b) case (ii), and (c) case (iii) defined in section 4.3.

noticable at high E/N ratios typical in the streamer head region. This is also demonstrated in (Liu and Pasko 2004, figure 1(a)) where calculated  $\nu_a$  values from (Morrow and Lowke 1997) and (Pasko *et al* 1999) are considerably different. Values for  $\nu_a$  and  $\nu_i$  obtained from inputting (Phelps 2013) cross sections to BOLSIG+ are very similar to those calculated in (Pasko *et al* 1999).

4.4. The Photo-ion yield function of air  $\Psi$ 

The photo-ion yield function  $\Psi$  has been extensively used in all previous experimental studies of photoionization in air and therefore it is instrumental to put the present modeling in the context of related formulations. Therefore, in this section, we compare the photo-ion yield function of the new model with those already published in literature (Penney and Hummert 1970, Naidis 2006, Aints *et al* 2008). We note that the photo-ion yield function of the present work has been calculated in appendix B.

Using the model of Zheleznyak et al (1982), Naidis (2006) demonstrated that in a case when the photon propagator does not vary along the photo-ion collector, the photoion yield function becomes independent of the length  $\Delta R$  of the collector used in experimental settings (see appendix B). Here, we calculate  $\Psi$  for the general case where variations of  $g(p_{\Omega_0}R)$  over the collector length are not necessarily negligible. It is demonstrated that in this case  $\Psi$  becomes a function of the product  $p\Delta R$ , which as stated in (Penney and Hummert 1970) is proportional to the number of molecules a photon traverses through the collector length. Hence, smaller values of  $p\Delta R$  correspond to lower photoabsorption, which in turn results in negligible variations in  $g(p_{O_2}R)$  along the photo-ion collector. As a result, we expect our calculated photo-ion yield function for the model of Zheleznyak et al (1982), Y<sup>Z</sup>, to converge to the result obtained in (Naidis 2006) in the limit where  $pDR \boxtimes 0$  (see appendix B).



In order to quantify the variations of the photon propagator over the collector, we define a function  $y(p_0, R)$  as

$$y(p_{O_2}R) = \frac{1}{p_{O_2}DR} \grave{Q}_0^{p_{O_2}DR} g(p_{O_2}(R\phi + R)) d(p_{O_2}R\phi.$$
(19)

We note that by definition,  $y(p_{O_2}R)$  converges to  $g(p_{O_2}R)$  in the limit where  $pDR \boxtimes 0$ . In appendix B, we demonstrate that the function  $\Psi$  is directly related to  $y(p_0, R)$ . In fact, (Qy) 1Y is only a function of the reduced electric field and therefore determines the contribution of emission intensity to the photo-ion yield function, while  $y(p_0, R)$  quantifies the contribution of  $g(p_0, R)$ . The quantity  $y(p_0, R)$  has been calculated in appendix B for the present work. Figure 9 depicts  $y(p_{O_2}R)/g(p_{O_2}R)$  for the present work. As seen in this figure, at low  $p_{O_2}R$  values  $y(p_{O_2}R)$  and consequently the photo-ion yield function change significantly as a function of pDR. In other words, the photo-ion yield function varies as a function of the collector length. In order to avoid this issue, the collector should be located at a distance R from the source at which the dimensions of the collector do not affect the result of the experiment. Also, for a constant collector length, the highest pressure at which photo-ion yield measurements may be performed must be limited such that at a desired  $p_{O_2}R$ ,  $p_{O_2}DR$  does not modify the measurement results. Ideal scenario from this stand point is to minimize the detector length DR. Note that pDR in photo-ion yield measurements of Penney and Hummert (1970) and Aints et al (2008) attains values as high as 36 and 42 Torr cm, respectively. Results presented in figure 9 may be interpreted as a correction factor through which the finite-length effect of the collector is removed from experimental results, especially at low  $p_{\Omega_0}R$ values.

The effect depicted in figure 9 for low  $p_{O_2}R$  values may be explained using the fits to the photon propagator function.

From table 1, it is seen that the fits introduce a number of photoabsorption scales  $(l_i p_{\Omega_2})^{-1}$  which govern the damping behavior of the photon propagator. At large distances from the source, the terms with higher photoabsorption coefficients  $l_i p_{\Omega_2}$  reduce significantly and terms with lower photoabsorption coefficients contribute to  $g(p_{O_2}R)$  the most. Since the photoabsorption scale of the remaining terms is large compared to DR, one can assume that  $g(p_0, R)$  will not vary significantly through the collector length and therefore, the assumption that  $g(p_{0}, R)$  is constant over the collector is valid. As a result,  $\Psi$  becomes independent from the collector dimensions. On the other hand, once we approach the source of radiation (lower  $p_{\Omega}$ , R values), the contribution from terms with photoabsorption scales comparable to DR increases and therefore  $g(p_0, R)$  varies considerably over the collector length. Consequently,  $\Psi$  becomes dependent on the collector dimensions.

By definition, the photo-ion yield function varies as a function of the quenching factor Q, which includes pressure p as an individual variable (see appendix B). Following Naidis (2006) and Aints et al (2008), we introduce the quantity  $Q^{-1}Y$ in order to remove direct dependence of the photo-ion yield function on pressure through quenching. As a result, pressure manifests itself in  $Q^{-1}Y$  only through the terms pR and pDR. Figure 10(a) depicts  $Q^{-1}Y$  for the present work in the limit where  $pDR \boxtimes 0$ . It also includes  $Q^{-1}Y$  for the model of Zheleznyak et al (1982), and a modified version of the model of Zheleznyak et al (1982) due to Aints et al (2008), where based on experimental results, the authors suggest the updated value  $c_{\min} = 0.028 \text{ Torr}^{-1} \text{ cm}^{-1}$  as opposed to the original value  $c_{\min} = 0.035 \text{ Torr}^{-1} \text{ cm}^{-1}$  (see appendix A) in order to better match  $\Psi$  calculated using the model of Zheleznyak et al (1982) with long range experimental values. These representative calculations are performed for  $E/p = 210.5 \text{ V cm}^{-1} \text{ Torr}^{-1}$ , which corresponds to E/N = 595 Td ( $E = 160 \,\text{kV cm}^{-1}$ ,  $N = N_0 = 2.688$  '  $10^{25}$  m<sup>-3</sup>, where  $N_0$  denotes air density at ground pressure) and therefore,  $\overline{x_{0}^{Z}}w/a$   $\boxed{8}0.05$  in case of the model of Zheleznyak et al (1982) (see appendix A for definition of  $\omega$  and  $\alpha$ ). Since W/a varies slowly as a function of E/N, we do not expect major modifications in results depicted in figure 10(a) at other reduced electric fields. As a result, we depict results corresponding to a single E/N ratio.

Experimental results of Penney and Hummert (1970) and Aints *et al* (2008) have not been included in figure 10(a) since it has already been established that the model of Zheleznyak *et al* (1982) is in satisfactory agreement with those works (see e.g. Pancheshnyi 2015, figure 16). At most  $p_{O_2}R$  values, the results of the present work are also consistent with results obtained from the original and modified model of Zheleznyak *et al* (1982). While numerical values appear to be different by a factor of 2 to 3 at pR 300 Torr cm, they coincide with previous results at low pR 10 Torr cm and high pR 700 Torr cm values. Assuming constant pressure, the difference observed in the slope of the plots in figure 10(a) is merely due to the interplay of  $N_2$  emission spectra and photoabsorption due to air molecules. Note that at constant

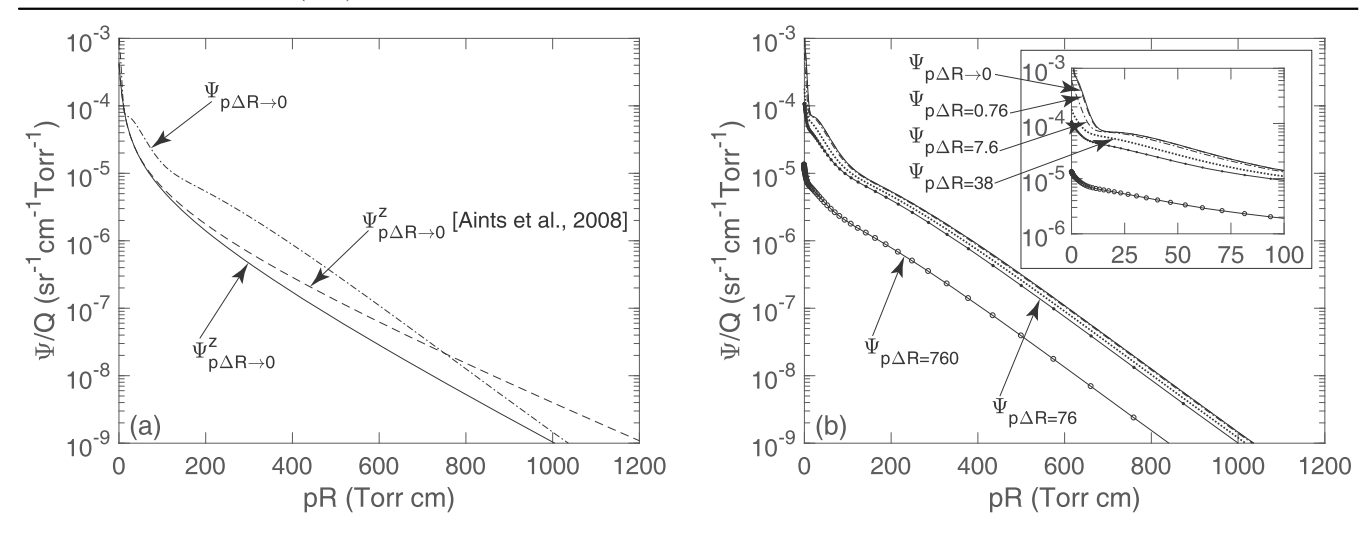


**Figure 10.** (a) The function  $\Psi/Q$  calculated at E/N=595 Td for the present work, the model of Zheleznyak *et al* (1982), and a modified version of the model of Zheleznyak *et al* (1982) due to Aints *et al* (2008) in the limit where  $pDR \boxtimes 0$  and (b) the function  $\Psi/Q$  calculated at E/N=595 Td for the present work in the limit where  $pDR \boxtimes 0$  and for  $p\Delta R=0.76$ , 7.6, 38, 76, 760 Torr cm.

pressure,  $(Qy)^{-1}Y$  is only a function of electric field (see equations (B.13) and (B.15)). That is, variations in the ratio W/a only cause vertical shifts in the plots in figure 10(a) since if  $(Qy)^{-1}Y = f(E)$  where f is an arbitrary function, one arrives at  $Q^{-1}Y = f(E)y(p_{O_2}R)$ . We emphasize that the measured XUV spectra of  $N_2$  along with  $N_2$  and  $O_2$  photoabsorption cross sections used in this work are significantly different from the approximations employed in the model of Zheleznyak et al (1982). In spite of fundamental issues arising from approximations made in the model of Zheleznyak et al (1982), this model is nevertheless in satisfactory agreement with experiments. As already mentioned (i) absence of electron impact excitation frequencies of certain rovibrational levels of N<sub>2</sub> calculated using the electron energy distribution function in air and consequently (ii) lack of a modeled XUV spectra for N<sub>2</sub> resulting from nonthermal discharges in air have hampered a more accurate modeling of the photo-ion yield function. We note that in comparing experimental results with the photo-ion yield function of the present model one should account for the finite-length effect of the collector reducing  $y(p_{O_2}R)$  compared to  $g(p_{O_2}R)$  at low  $p_{O_2}R$  values (see figure 9). Experimental results correspond to  $y(p_{\Omega_0}R)$ for finite  $p\Delta R$  values.

Figure 10(b) depicts the photo-ion yield function of the present work for various  $p\Delta R$  values. The numerical values for  $p\Delta R$  have been chosen according to experimental values of  $\Psi$  published in (Penney and Hummert 1970) and (Aints et al 2008), where the collector length is  $\Delta R=2$  and 0.056 cm, respectively. In particular,

- $p\Delta R = 0.76$  Torr cm approximately corresponds to  $(p, \Delta R) = (0.4 \text{ Torr}, 2 \text{ cm})$  in (Penney and Hummert 1970) and  $(p, \Delta R) = (20 \text{ Torr}, 0.056 \text{ cm})$  in (Aints *et al* 2008).
- pDR = 38 Torr cm approximately corresponds to  $(p, \Delta R) = (18 \text{ Torr}, 2 \text{ cm})$  in (Penney and Hummert 1970) and  $(p, \Delta R) = (760 \text{ Torr}, 0.056 \text{ cm})$  in (Aints *et al* 2008).

As inferred from this figure,  $Q^{-1}\Psi$  functions corresponding to  $p\Delta R\leqslant 100\,$  Torr cm are essentially the same with minor

deviations at low pR values. On the other hand, as  $p\Delta R$  grows to 760 Torr cm, significant reduction is observed in  $Q^{-1}\Psi$ , especially at lower pR values. Therefore, in interpretation of measurements, one should consider the effect of the finite length of the collector on results, especially at high  $p\Delta R$  and low pR values.

5. Conclusions

In this paper, we introduce a general framework for photoionization calculations and revisit the problem of photoionization of  $O_2$  in air due to nonthermal gas discharges. In particular, we distinguish certain high energy singlet states of  $N_2$  as the source of high energy photons capable of photoionizing  $O_2$ , calculate the density of  $N_2$  molecules transitioning to these states due to electron impact using their electron impact excitation cross sections, and quantify the source of radiation upon spontaneous emission of photons from these states. Photoabsorption in air is modeled using experimental values for the photoabsorption cross section of  $N_2$  and  $O_2$  in the entire spectral range of emission aforementioned.

Furthermore, the current most widely used photoionization model in air due to Zheleznyak  $et\ al\ (1982)$  is discussed and its limitations are outlined. We provide improvements for each of the limitations. In particular, we use experimental values for the photoabsorption cross section of  $O_2$  as opposed to the analytical function used in (Zheleznyak  $et\ al\ 1982$ ) to approximate the photobabsorption cross section of  $O_2$ . In addition, we account for the contribution of  $O_2$  to photoabsorption through the entire spectrum of emission.

The presented photoionization model is compared with the model of Zheleznyak et~al~(1982) through numerical examples and the photo-ion yield function  $\Psi$  that was commonly used in previous experimental work for the quantitative characterization of photoionization. It is demonstrated that the two models produce similar results in both cases.

Finally, it is demonstrated that gas discharge phenomena, in particular streamers, manifest similar properties upon application of both photoionization models.

#### **Acknowledgments**

This research was supported by NSF under AGS-1623780 and AGS-1744099 grants to Penn State University.

## Appendix A. Derivation of the model of Zheleznyak et al (1982) from the general photoionization framework

In the original photoionization model proposed by Zheleznyak *et al* (1982), photoionization calculations for  $O_2$  include effects only in the 98–102.5 nm interval. The lower bound is set to 98 nm below which heavy absorption of photons would occur by  $N_2$  in addition to  $O_2$  (figure A1(b)) and the upper bound is due to the fact that photons with wavelengths longer than 102.5 nm may get absorbed by  $O_2$  but are not energetic enough to cause photoionization of  $O_2$  (figure A1(a)). As a result, photons with wavelengths in the range 98–102.5 nm will get absorbed exclusively by  $O_2$  and consequently photoionize  $O_2$ .

The purpose of this section is to derive the model of Zheleznyak *et al* (1982) in terms of the general photo-ionization framework described in the main text of this paper.

The photoionization rate per a single molecule of  $O_2$  per unit volume,  $S_{ph_1}^Z(F)$  may be written in the form consistent with the model of Zheleznyak *et al* (1982) as:

$$S_{\mathrm{ph}_{1}}^{Z}(\vec{r}) = \grave{Q}_{\psi} \tilde{I}^{Z}(r \phi \frac{\aleph^{Z}(pR)}{4pR^{2}} \mathrm{d}V \not c \tag{A.1}$$

where

$$\begin{split} \tilde{g}^{Z}(pR) &= \grave{Q}_{\phi} s^{Z}(I \not \phi e^{-k\frac{Z}{Q_{2}}(I \not \phi R s} \overset{Z}{Q_{2}} ) (x) \not \phi \overset{Z}{Q_{2}} ) (I \not \phi f s) & \phi \\ &= \overline{\chi_{Q_{2}}^{Z}} \grave{Q}_{\phi} s^{Z}(I \not \phi e^{-k\frac{Z}{Q_{2}}(I \not \phi R s)} \overset{Z}{Q_{2}} ) (x) \not \phi f s) & \phi \end{split} \tag{A.2}$$

and

$$\tilde{I}^{Z}(\overrightarrow{p}) = \frac{p_{\rm q}}{p + p_{\rm q}} n^{Z \nabla h_{\rm e}}. \tag{A.3}$$

The superscript Z denotes quantities obtained following (Zheleznyak *et al* 1982) model formulation whenever used in this section. We note that (A.1) is of the same form as (7). Using (A.2) we convert (A.1) to the form agreeing with the model of Zheleznyak *et al* (1982):

$$S_{\mathrm{ph}_{1}}^{Z}(\overrightarrow{P}) = \grave{Q}_{\psi} I^{Z}(r) \stackrel{\mathbb{Z}^{2}(pR)}{4pR^{2}} dV \not c$$
 (A.4)

where

$$I^{Z}(\overrightarrow{P_{q}}) = \frac{p_{q}}{p + p_{q}} \overline{X_{O_{2}}^{Z}} \frac{n^{Z} \overline{M}}{n_{i}} n_{i} n_{e} = \frac{p_{q}}{p + p_{q}} \overline{X_{O_{2}}^{Z}} \frac{n^{Z} \overline{M}}{n_{i}} S_{i} \quad (A.5)$$

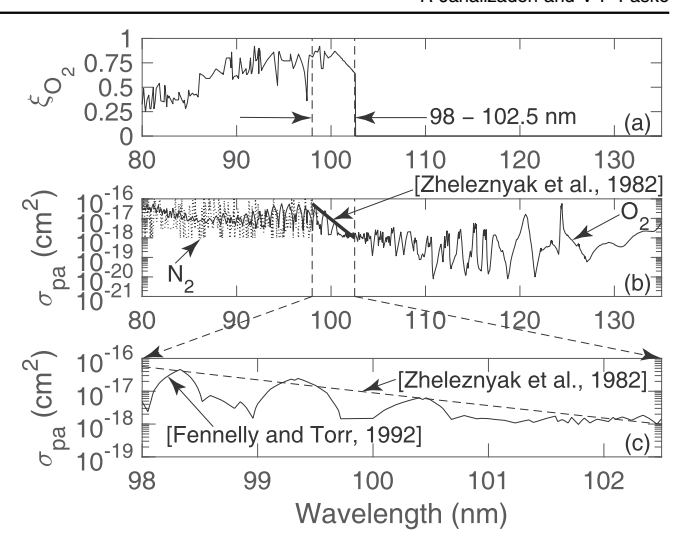


**Figure A1.** (a) Photoionization probability or photoionization yield of  $O_2$  in the XUV range (Fennelly and Torr 1992), (b) Photoabsorption cross sections of  $O_2$  and  $N_2$  (Fennelly and Torr 1992) in addition to the approximation of Zheleznyak *et al* (1982), and (c) a zoomed in version of (b).

and

$$g^{Z}(pR) = \grave{Q}_{\phi} s^{Z}(l \phi e^{-k_{O_{2}}^{Z}(l \phi R)} \grave{S}_{O_{2}}^{Z} l) kd \phi$$
 (A.6)

denote intensity and the photon propagator, respectively. From (A.2), (A.3), (A.5), (A.6) we readily conclude that  $\tilde{g}^Z = \overline{\chi}_{0_2}^Z g^Z$  and  $\tilde{I}^Z = I^Z/\overline{\chi}_{0_2}^Z$ , and therefore  $I^Z g^Z = \tilde{I}^Z \tilde{g}^Z$ . The quantity  $\overline{\chi}_{0_2}^Z$  denotes the average photoionization yield of  $O_2$  in the 98–102.5 nm interval and  $S_i = n_i n_e$  denotes the number of ionization events per unit volume per unit time. In the model of Zheleznyak *et al* (1982) and most related previous works (e.g. Naidis 2006, Pancheshnyi 2015), the fraction  $n^{Z[X]}/n_i$  is denoted by  $\omega/\alpha$  where  $w = n^{Z[X]}/v_{dr}$  denotes the excitation coefficient of the radiating states of  $N_2$  molecules due to electron impact,  $a = n_i/v_{dr}$  is the ionization coefficient, and the quantity  $v_{dr}$  is the magnitude of the drift velocity of electrons. In addition, the photoabsorption cross section of  $O_2$ ,  $S_{O_2}^Z$ , in the 98–102.5 nm interval is approximated by a sharp function of wavelength of the form (Mnatsakanyan and Naidis 1991):

$$\mathbf{s}_{O_2}^Z = \mathbf{s}_0 \left( \frac{\mathbf{c}_{\text{max}}}{\mathbf{c}_{\text{min}}} \right)^{\frac{I-I_1}{I_2-I_1}},$$
 (A.7)

where  $s_0 = 9.8958$  ′  $10^{-19}$  cm²,  $c_{max} = 2$  Torr¹ cm¹,  $\chi_{min} = 0.035$  Torr¹ cm¹,  $\lambda_1 = 102.5$  nm and  $\lambda_2 = 98$  nm. We note that in the original modeling (Zheleznyak *et al* 1982, Mnatsakanyan and Naidis 1991) the cross section approximation of the type (A.7) is performed in frequency space. However, as can be easily verified and shown below, the approximation (A.7) in wavelength space is essentially the same and leads to identical results. Figure A1(c) compares the approximation to the photoionization cross section of O<sub>2</sub> utilized in (Zheleznyak *et al* 1982) with experimental data compiled by (Fennelly and Torr 1992). As inferred from this figure, the approximation of Zheleznyak *et al* (1982) does not

capture the complex structure of the photoabsorption cross section of O<sub>2</sub>. The same argument holds for the approximated spectrum of photoionizing emission from N2, which is assumed to be the constant value  $s^{Z}(I) = 1/(1-I)$  and limited to the same interval. We note that  $\grave{o}^{l_1} s^{\mathbb{Z}}(l \not o d \not = 1)$ . Having substituted (A.7) in (A.6) we arrive at

$$\frac{g^{Z}(p_{O_{2}}R)}{p_{O_{2}}R} = g_{0}\frac{\exp(-c_{\min}p_{O_{2}}R) - \exp(-c_{\max}p_{O_{2}}R)}{(p_{O_{2}}R)^{2}\ln\left(\frac{c_{\max}}{c_{\min}}\right)} \tag{A.8}$$

for the photon propagator of the model of Zheleznyak et al (1982), where  $g_0 = p_{O_2}/n_{O_2} = 2.8274$  '  $10^{-17}$  Torr cm<sup>3</sup>.

Once we quantify the source of radiation in the model of Zheleznyak et al (1982), the integral representation (A.4) may be used to calculate the photoionization rate of O<sub>2</sub> in air using this model. We emphasize that in (A.5) the quantity  $x_{0}^{Z}$   $n^{Z} / n_{i}$  collectively contributes to the source of radiation (as opposed to our model in which  $x_{O_2}$  is embedded in the photon propagator, while  $n^{|M|}$  individually contributes to the source of radiation). The quantity  $\overline{X_{0}^{Z}} n^{Z} \sqrt[M]{n_i}$  is provided in (Zheleznyak et al 1982) as a function of the reduced electric field and in tabular format (see table 2). As a result, one can use (A.5) in combination with (A.8) to implement the photoionization model of Zheleznyak et al (1982) in integral form. Furthermore, transforming the integral representation of the model of Zheleznyak et al (1982) to a set of differential equations has already been discussed elsewhere (e.g. Bourdon et al 2007) in great detail.

#### Appendix B. Calculation of the photo-ion yield function $\Psi$

In this appendix we provide connection of modeling reported in present work with previous experimental studies of photoionization in air that are commonly expressed in terms of the photo-ion yield function,  $\Psi$ . As described in (e.g. Naidis 2006, Aints et al 2008),  $\Psi$  denotes the number of photo-ions generated in a layer of unit thickness at a distance R from the radiation source at unit pressure per unit solid angle per one ionizing collision in a discharge. We assume the discharge occurs in a volume  $V_1$  and calculate the number of photo-ions generated in a volume  $V_2$  per unit time. Following the notation in (Naidis 2006), the number of electron impact ionization events per unit time can be calculated as

$$\boxed{\mathbf{W}_{\text{on}} = \grave{\mathbf{Q}}_{i} a v_{\text{dr}} n_{\text{e}} dV_{\text{l}} = \grave{\mathbf{Q}}_{i} n_{\text{i}} n_{\text{e}} dV_{\text{l}} = \grave{\mathbf{Q}}_{i} S_{\text{i}} dV_{\text{l}}. \quad (B.1)}$$

Furthermore, the number of photons generated per unit time, i.e. in (Naidis 2006), can be expressed as

$$\mathbf{W} = \mathbf{\hat{Q}}_{l} I(\mathbf{r} \mathbf{\hat{\phi}} dV_{l}, \tag{B.2}$$

where  $I(\overrightarrow{r})$  may be written in the form

$$I(\overrightarrow{r} ) = \frac{p_{\mathbf{q}}}{p + p_{\mathbf{q}}} \overrightarrow{n} | \mathbf{M}_{e} = \frac{p_{\mathbf{q}}}{p + p_{\mathbf{q}}} \frac{\overrightarrow{n} | \mathbf{M}}{n_{\mathbf{i}}} n_{\mathbf{i}} n_{\mathbf{e}}$$

$$= \frac{p_{\mathbf{q}}}{p + p_{\mathbf{q}}} \frac{\overrightarrow{n} | \mathbf{M}}{n_{\mathbf{i}}} S_{\mathbf{i}} = \frac{p_{\mathbf{q}}}{p + p_{\mathbf{q}}} \frac{\mathbf{W}}{\mathbf{a}} S_{\mathbf{i}}. \tag{B.3}$$

As a result, (B.2) can be written in the form

$$\mathbf{W} = \frac{p_{\mathbf{q}}}{p + p_{\mathbf{q}}} \grave{\mathbf{Q}}_{V_{1}} \frac{\mathbf{w}}{\mathbf{a}} S_{\mathbf{i}} dV_{1} = \frac{p_{\mathbf{q}}}{p + p_{\mathbf{q}}} \frac{\mathbf{w}}{\mathbf{a}} \grave{\mathbf{Q}}_{\mathbf{i}} S_{\mathbf{i}} dV_{1}$$

$$= \frac{p_{\mathbf{q}}}{p + p_{\mathbf{q}}} \frac{\mathbf{w}}{\mathbf{a}} \mathbf{W}_{\text{on}}, \tag{B.4}$$

where it is assumed that  $\omega/\alpha$  varies weakly with the reduced electric field E/p over the discharge volume.

The number of photoionization events occurring in volume  $V_2$  per unit time due to arrival of photons generated as a result of the discharge occurring in volume  $V_1$  may be calculated as

$$\mathbf{W}_{\mathrm{ph}} = \mathbf{\hat{Q}}_{v_2} S_{\mathrm{ph}}(\mathbf{r}) \mathbf{d} V_2, \tag{B.5}$$

where  $S_{\rm ph}(r)$  may be written in the form

and  $n_{O_2}$  is the density of  $O_2$ . Combining (B.5) and (B.6), we arrive at  $\boxed{\mathbb{W}_{ph}} = n_{O_2} \grave{O}_{I} I(F ) \grave{O}_{I} \frac{g(p_{O_2}R)}{4nR^2} dV_2 dV_1. \tag{B.7}$ 

$$\mathbf{W}_{\text{ph}} = n_{\text{O}_2} \, \mathbf{\hat{Q}}_{V_1} \, I(\mathbf{F}_{\varphi}) \, \mathbf{\hat{Q}}_2 \, \frac{g(p_{\text{O}_2}R)}{4pR^2} dV_2 dV_1. \tag{B.7}$$

We can express a differential volume element in  $V_2$  as  $dV_2 = R^2 dR dV$  where  $d\Omega$  is a differential element of the solid angle as  $\frac{1}{N}$  result of looking towards  $V_2$  from  $V_1$  along the vector R. Subsequently, (B.7) can be written as

$$\begin{split} \boxed{\mathbb{M}_{\text{ph}}} &= n_{\mathrm{O}_{2}} \stackrel{\bullet}{\mathbf{O}}_{V_{1}} I(P \not P) \stackrel{\bullet}{\mathbf{O}}_{V_{1}} \stackrel{\bullet}{\mathbf{O}}_{V_{1}} \\ &\cdot \frac{g(p_{\mathrm{O}_{2}}R\phi)}{4pR\phi^{2}} R\phi^{2} dR \phi W \mathcal{L} V_{1} \\ &= \frac{W}{4p} n_{\mathrm{O}_{2}} \stackrel{\bullet}{\mathbf{O}}_{V_{1}} I(P \not P) \stackrel{\bullet}{\mathbf{O}}_{V_{1}} g(p_{\mathrm{O}_{2}}R) dR d\Phi V_{1}. \end{split} \tag{B.8}$$

Under the approximation that variations of the photon propagator are negligible from R to  $R + \Delta R$ , one arrives at

$$\mathbf{W}_{ph} = \frac{\mathbf{W}}{4n} \mathbf{W}_{O_2} g(p_{O_2} R) \mathsf{D} R \tag{B.9}$$

and subsequently.

$$Y = \frac{1}{pWDR} \frac{\mathbb{W}_{ph}}{\mathbb{W}_{on}} = \frac{1}{20pg_0} \frac{p_q}{p + p_q} \frac{w}{a} g(p_{O_2}R), \quad (B.10)$$

where we have used the fact that in air  $p_{\rm O_2}$  = 0.2p and  $g_0 = p_{O_2}/n_{O_2}$  as defined in appendix A. In an experimental setting (e.g. Aints et al 2008, Penney and Hummert 1970)  $\Delta R$  denotes the length of the collector region in which photoionizing current is measured and  $\Omega$  is the solid angle

spanned by the collector. From (B.10) it is inferred that in case of negligible variations of the photon propagator along the collector region,  $\Psi$  is independent of the collector dimensions.

The equation (B.10) has been derived for the model of Zheleznyak *et al* (1982) in (Naidis 2006) using the aforementioned approximation. Here, however, we calculate  $\Psi$  in a general form assuming that the variation of the photon propagator from R to  $R + \Delta R$  is not necessarily negligible. In other words, we analytically calculate (B.8) for the photon propagator function of both the present work and the model of Zheleznyak *et al* (1982). Modifying (B.10) in order to account for the variations of  $g(p_0, R)$  over the collector, we arrive at

$$Y = \frac{1}{20pg_0} \frac{p_q}{p + p_0} \frac{w}{a} Y,$$
 (B.11)

where

$$y = \frac{1}{p_{O_2} DR} \grave{Q}_0^{p_{O_2} DR} g(p_{O_2} (R \not c + R)) d(p_{O_2} R \not c). \quad (B.12)$$

We note that  $\psi$  measures the dependence of the photo-ion yield on the collector length and reduces to  $g(p_{O_2}R)$  in case of constant  $g(p_{O_2}R)$  or in the limit where  $p_{O_2}DR \boxtimes 0$ .

Using the exponential integral defined as  $E_1(x) = \delta_x^* \frac{e^{-t}}{t} dt$ , the photo-ion yield function of the model of Zheleznyak *et al* (1982) may be written as

where

$$\frac{\mathsf{Y}^{\mathsf{Z}}}{Q} = \frac{1}{20pg_0} \frac{\mathsf{w}}{\mathsf{a}} \mathsf{y}^{\mathsf{Z}},\tag{B.13}$$

and  $b_i = l_i p_{O_2} R$  and  $Db_i = l_i p_{O_2} DR$ . Related distributions for a range of pDR values are illustrated in figures 9 and 10(b). Similar to the case of  $y^Z$ , (B.16) converges to the photon propagator of the present work in the limit where  $p_{O_2}DR \times 0$ .

#### **ORCID iDs**

R Janalizadeh https://orcid.org/0000-0002-6014-2671

#### References

Aints M, Haljaste A, Plank T and Roots L 2008 Absorption of photo-ionizing radiation of corona discharges in air *Plasma Process. Polym.* 5 672–80

Ajello J M, James G K, Franklin B O and Shemansky D E 1989 Medium-resolution studies of extreme ultraviolet emission from  $N_2$  by electron impact: Vibrational perturbations and cross sections of the  $c \not \in S_u^+$  and  $b \not \in S_u^+$  states *Phys. Rev.* A 40 3524–56

Ajello J M, Stevens M H, Stewart I, Larsen K, Esposito L, Colwell J, McClintock W, Holsclaw G, Gustin J and Pryor W 2007 Titan airglow spectra from Cassini ultraviolet imaging spectrograph UVIS): EUV analysis *Geophys. Res.* Lett. 34 L24204

Bagheri B et al 2018 Comparison of six simulation codes for positive streamers in air Plasma Sources Sci. Technol. 27 095002

Barrington-Leigh C P, Inan U S and Stanley M 2001 Identification of sprites and elves with intensified video and broadband array photometry *J. Geophys. Res.: Space Phys.* **106** 1741–50 Bourdon A, Pasko V P, Liu N Y, Célestin S, Ségur P and Marode E

2007 Efficient models for photoionization produced by non-

$$y^{Z} = \frac{g_{0}}{\ln\left(\frac{c_{\max}}{c_{\min}}\right)} \frac{([E_{1}(b_{\min}) - E_{1}(b_{\min} + D b_{\min})] \quad [E_{1}(b_{\max}) \quad E_{1}(b_{\max}) \quad b_{\max})])}{p_{O_{2}}DR}$$
(B.14)

and  $b_{\min} = c_{\min} p_{O_2} R$ ,  $Db_{\min} = c_{\min} p_{O_2} DR$ ,  $b_{\max} = c_{\max} p_{O_2} R$ ,  $Db_{\max} = c_{\max} p_{O_2} DR$ . The quantity  $Y^Z/Q$  is not a function of only pressure, but varies according to the product  $p_{O_2} DR$  at a certain  $p_{O_2} R$  and E/N value. In the limit where  $p_{O_2} DR \boxtimes 0$ , (B.14) reduces to  $g^Z(p_{O_2} R)$  as defined in (A.8). Performing the same calculation for the photon propagator function of the present work using the 6-exponent fit, we arrive at

$$\frac{\mathsf{Y}}{O} = \frac{1}{20pq_0} \frac{\mathsf{w}}{\mathsf{a}} \mathsf{y},\tag{B.15}$$

where

$$y = \frac{1}{p_{\mathrm{O}_2} \mathsf{D} R} \, \mathring{\mathbf{a}}_i \, \, \frac{C_i}{l_i^2} \mathrm{e}^{-\,b_i} ((1 + b_i) - \,\, \bar{\mathrm{e}}^{\mathsf{D} - b_i} (1 + \,\, b_i)).$$

(B.16)

thermal gas discharges in air based on radiative transfer and the Helmholtz equations *Plasma Sources Sci. Technol.* **16** 656–78 Dhali S K and Williams P F 1987 Two-dimensional studies of

streamers in gases *J. Appl. Phys.* **62** 4696–707

Dirac P A M 1948 *The Principles of Quantum Mechanics* (Oxford: Oxford University Press)

Fennelly J A and Torr D G 1992 Photoionization and photoabsorption cross sections of O, N<sub>2</sub>, O<sub>2</sub>, and N for aeronomic calculations *At. Data Nucl. Data Tables* **51** 363

Franz R C, Nemzek R J and Winckler J R 1990 Television image of a large upward electric discharge above a thunderstorm system *Science* **249** 48

Frey H et al 2007 Halos generated by negative cloud-to-ground lightning Geophys. Res. Lett. 34 L18801

Hagelaar G J M and Pitchford L C 2005 Solving the Boltzmann equation to obtain electron transport coefficients and rate coefficients for fluid models *Plasma Sources Sci. Technol.* 14 722–33

Heays A N 2011 Photoabsorption and photodissociation in molecular nitrogen *PhD Thesis* The Australian National University

- Heays A N 2018 private communication
- Heays A N, Lewis B, Gibson S, Malone C, Johnson P, Kanik I and Khakoo M 2012 Tuning out vibrational levels in molecular electron energy-loss spectra *Phys. Rev.* A **85** 012705
- Heays A N, Ajello J M, Aguilar A, Lewis B R and Gibson S T 2014 The high resolution extreme ultraviolet spectrum of N<sub>2</sub> by electron impact *Astrophys. J. Suppl. Ser.* **211** 28
- Hockney R W and Eastwood J W 1988 Computer Simulation Using Particles (New York: McGraw-Hill)
- Hudson R D 1971 Critical review of ultraviolet photoabsorption cross sections for molecules of astrophysical and aeronomic interest Rev. Geophys. 9 305–406
- Itikawa Y 2006 Cross sections for electron collisions with nitrogen molecules J. Phys. Chem. Ref. Data 35 31–53
- James G K, Ajello J M, Franklin B and Shemansky D E 1990 Medium resolution studies of extreme ultraviolet emission from N<sub>2</sub> by electron impact: the effect of predissociation on the emission cross section of the b<sup>1</sup>P<sub>u</sub> state J. Phys. B: At. Mol. Opt. Phys. 23 2055–81
- Janalizadeh R and Pasko V P 2019a Photoionization and electron impact ionization of metallic species at sprite altitudes as a mechanism of initiation of sprite streamers CEDAR MLT Poster Session Booklet (Santa Fe, NM, 16-21 June 2019) p 42 Abstract SPRT-01
- Janalizadeh R and Pasko V P 2019b Photoionization and electron impact ionization of metallic species at sprite altitudes as a mechanism of initiation of sprite streamers Abstract PO18PM-020 presented at XXXIV ICPIG & ICRP-10 (Sapporo, Hokkaido, 14-19 July 2019)
- Keller-Rudek H, Moortgat G K, Sander R and Sörensen R 2013 The MPI-Mainz UV/VIS spectral atlas of gaseous molecules of atmospheric interest *Earth Syst. Sci. Data* **5** 365–73
- Khakoo M A, Malone C P, Johnson P V, Lewis B R, Laher R, Wang S, Swaminathan V, Nuyujukian D and Kanik I 2008 Electron-impact excitation of  $X^1S_g^*(v^{\phi \phi} = 0)$  to the  $a^{\bullet \phi}_g^*$ ,  $b^1P_u$ ,  $c_3^1P_u$ ,  $o_3^1P_u$ ,  $b\phi S_u^*$ ,  $c\phi S_u^*$ ,  $G^3P_u$ , and  $F^3P_u$  states of molecular nitrogen *Phys. Rev.* A 77 012704
- Kulikovsky A A 1997 Positive streamer between parallel plate electrodes in atmospheric pressure air *J. Phys. D: Appl. Phys.* **30** 441–50
- Liu N Y and Pasko V P 2004 Effects of photoionization on propagation and branching of positive and negative streamers in sprites J. Geophys. Res. 109 A04301
- Lofthus A and Krupenie P H 1977 The spectrum of molecular nitrogen *J. Phys. Chem. Ref. Data* 6 113–307
- Luque A, Ebert U, Montijn C and Hundsdorfer W 2007 Photoionization in negative streamers: Fast computations and two propagation modes Appl. Phys. Lett. 90 081501
- Malone C P, Johnson P V, Liu X, Ajdari B, Kanik I and Khakoo M A 2012 Integral cross sections for the electron-impact excitation of the  $b^1P_u$ ,  $c_3^1P_u$ ,  $o_3^1P_u$ ,  $b_{\psi}^{\dagger}S_u^{\dagger}$ ,  $c_{\psi}^{\dagger}S_u^{\dagger}$ ,  $G^3P_u$ , and  $F^3P_u$  states of N<sub>2</sub> Phys. Rev. A 85 062704
- McHarg M G, Stenbaek-Nielsen H C and Kammae T 2007 Streamer development in sprites *Geophys. Res. Lett.* **34** L06804
- Mignone A 2014 High-order conservative reconstruction schemes for finite volume methods in cylindrical and spherical coordinates *J. Comput. Phys.* **270** 814
- Mnatsakanyan A K and Naidis G V 1991 Charged particle production and loss processes in nitrogen-oxygen plasmas *Reviews of Plasma Chemistry* ed B M Smirnov vol 1 (New York: Consultants Bureau)
- Morrow R and Lowke J J 1997 Streamer propagation in air *J. Phys. D: Appl. Phys.* **30** 614–27
- Moss G D, Pasko V P, Liu N Y and Veronis G 2006 Monte Carlo model for analysis of thermal runaway electrons in streamer tips in transient luminous events and streamer zones of lightning leaders J. Geophys. Res. 111 A02307

- Naidis G V 2006 On photoionization produced by discharges in air Plasma Sources Sci. Technol. 15 253–5
- Pai D Z, Lacoste D A and Laux C O 2010 Nanosecond repetitively pulsed discharges in air at atmospheric pressure-the spark regime *Plasma Sources Sci. Technol.* 19 065015
- Pancheshnyi S 2015 Photoionization produced by low-current discharges in O<sub>2</sub>, air, N<sub>2</sub> and CO<sub>2</sub> *Plasma Sources Sci. Technol.* **24** 015023
- Pancheshnyi S, Biagi S, Bordage M C, Hagelaar G J M, Morgan W L, Phelps A V and Pitchford L C 2012 The LXCat project: Electron scattering cross sections and swarm parameters for low temperature plasma modeling *Chem. Phys.* **398** 148–53
- Pasko V P 2018 Photoionization of metallic species at sprite altitudes by far-UV emissions of LBH band system of molecular nitrogen *Abstract AE21B-3132 presented at 2018 Fall Meeting, AGU (Washington, DC, 10–14 December 2018)*
- Pasko V P, Inan U S and Bell T F 1999 Thermal runaway electrons in sprites 1999 URSI National Radio Science Meeting, Program and Abstract (Boulder, CO, 4–8 January 1999) p 152
- Pasko V P, Qin J and Celestin S 2013 Toward better understanding of sprite streamers: Initiation, morphology, and polarity asymmetry *Surv. Geophys.* **34** 797–830
- Penney G W and Hummert G T 1970 Photoionization measurements in air, oxygen, and nitrogen *J. Appl. Phys.* **41** 572–7
- Potter D 1973 Computational Physics (New York: Wiley)
- Qin J and Pasko V P 2015 Dynamics of sprite streamers in varying air density Geophys. Res. Lett. 42 2031–6
- Roncin J-Y and Launay F 1998 Tables of vacuum ultraviolet emission band systems of molecular nitrogen from 82.6 to 124.2 nm *Astron. Astrophys. Suppl. Ser.* 128 361–2
- Ségur P, Bourdon A, Marode E, Bessières D and Paillol J H 2006 The use of an improved Eddington approximation to facilitate the calculation of photoionization in streamer discharges *Plasma Sources Sci. Technol.* **15** 648–60
- Sipler D P and Biondi M A 1972 Measurements of O(\(^1D\)) quenching rates in the F region *J. Geophys. Res.* 77 6202–12
- Sprengers J P 2006 Extreme ultraviolet laser excitation of molecular nitrogen: Perturbations and predissociation *PhD Thesis* Vrije Universiteit Amsterdam
- Stenbaek-Nielsen H, Kanmae T, McHarg M and Haaland R 2013 High-speed observations of sprite streamers *Surv. Geophys.* **34** 769–95
- Stephens J, Fierro A, Beeson S, Laity G, Trienekens D, Joshi R P, Dickens J and Neuber A 2016 Photoionization capable, extreme and vacuum ultraviolet emission in developing low temperature plasmas in air *Plasma Sources Sci. Technol.* **25** 025024
- Teich T H 1967 Emission gasionisierender strahlung aus electronenlawinen: I. Meß anordnung und Meß verfahren. Messungen in Sauerstoff *Z. Phys.* **199** 378–94
- Vallance-Jones A V 1974 *Aurora* (Norwell, Mass: D. Reidel Publishing Co.)
- Vitello P A, Penetrante B M and Bardsley J N 1994 Simulation of negative-streamer dynamics in nitrogen *Phys. Rev.* E 49 5574–98
- Walter C W, Cosby P C and Helm H 1994 Predissociation quantum yields of singlet nitrogen *Phys. Rev.* A **50** 2930–6
- Wilson C T R 1925 The electric field of a thundercloud and some of its effects *Proc. Phys. Soc.* 37 32D
- Xiong Z and Kushner M J 2014 Branching and path-deviation of positive streamers resulting from statistical photon transport *Plasma Sources Sci. Technol.* **23** 065041
- Zheleznyak M B, Mnatsakanyan A K and Sizykh S V 1982 Photoionization of nitrogen and oxygen mixtures by radiation from a gas discharge *High Temp.* **20** 357–62